Research article

Hydrostatic pressure-induced transformations and multifunctional properties of Francium-based halide perovskite FrCaCl$_3$: Insights from first-principles calculations

Md Istiaque Ahmed [a], Arpon Biswas [a], Tariqul Islam Asif [a], Md Saiduzzaman [a,**], Minhajul Islam [b,*]

[a] *Department of Materials Science and Engineering, Khulna University of Engineering & Technology (KUET), Khulna, 9203, Bangladesh*
[b] *Bangladesh Atomic Energy Regulatory Authority (BAERA), E-12/A, Agargaon, Dhaka, 1207, Bangladesh*

ABSTRACT

Under varying hydrostatic pressures ranging from 0 to 150 GPa, first-principles calculations were conducted to investigate the structural, electronic, bonding, optical, elastic, and mechanical characteristics of the Lead (Pb)-free halide perovskite FrCaCl$_3$ using both the GGA and hybrid HSE06 parameterized density functional theory (DFT). Since the FrCaCl$_3$ cubic perovskite has not yet been synthesized experimentally, its structural and thermodynamic stabilities are confirmed by the Goldschmidt tolerance factor, the octahedral factor, and the formation energy. The induction of pressure has caused a simultaneous decrease in both the lattice parameters and the electronic band gap. Applying the hybrid HSE06 potential refines the accuracy of the band gap, with values decreasing from 5.705 to 2.618 eV from 0 to 150 GPa pressure, suggesting improved optoelectronic attributes. Employing pressure facilitates the formation of stronger chemical bonds characterized by reduced bond lengths. The investigation of optical functions demonstrates that with increased pressure ranging to 150 GPa, the optical conductivity along with the absorption coefficient is oriented towards the low-energy region. The FrCaCl$_3$ perovskite has the prospect to be used in X-ray imaging and other fields of nuclear medicine and diagnostics as it contains the radioactive element Francium (Fr). Additionally, it is found via the study of mechanical characteristics that FrCaCl$_3$ is mechanically stable under various applied pressure, and adding pressure makes it more ductile as well as more anisotropic.

1. Introduction

Global industrialization has resulted in unprecedented increases in energy consumption, which mainly originates from non-renewable sources. The utilization of traditional fossil fuels along with hydrocarbons is linked to major environmental difficulties due to CO$_2$ emissions. Solar energy, on the other hand, is the most ubiquitous and environmentally beneficial energy source. Researchers and scientists are striving to create affordable, efficient, and eco-friendly photovoltaic cells to make the best utilization of natural resources. In this respect, owing to its versatile optical properties, perovskite materials have recently substantiated significant

potential in optoelectronic applications [1–6]. The cubic perovskites' general formula is ABX$_3$, where X is considered the anion (Oxygen or Halogens), on the other hand, A and B are the cations [7,8]. Despite their significant potential for photoluminescence applications, compounds containing Lead (Pb) are poisonous and hazardous [9,10]. Non-conventional Lead-free halide perovskites have the potential to capture the interest of scientific communities [11–16]. Therefore, a wide range of physical characteristics, such as structural, electronic, photonic, optical, and mechanical properties, is being thoroughly explored to better understand the challenges surrounding material utilization.

The physical attribute of material is typically examined using both computational and experimental methods to predict its applications [17–28]. A material's physical qualities are perhaps influenced by its structure. Perovskite is considered one of the significant materials among several kinds of crystalline structures [29–31] since it is typically composed of conductors, insulators, semiconductors, and superconductors [32–36]. Physical characteristics of the perovskite-type family include photocatalysis, ferroelectricity, pyroelectricity, piezoelectricity, magneticity, superconductivity, and ionic conductance [37–42]. Engaging in experimental investigations demands substantial time and financial resources, necessitating access to well-equipped laboratory facilities. In contrast, computational studies employing computer simulation methods offer a more cost-effective and relatively simpler approach. Computational research not only serves as a practical substitute but also lays a foundation for subsequent experimental investigations. Among the array of simulation methods available, Density Functional Theory (DFT) stands out as an exceptional tool for probing a diverse range of physical properties in materials. DFT-based first-principles computations have been carried out to examine several physical characteristics of cubic perovskite compounds [43–51].

The physical properties of a material can be altered through the application of hydrostatic pressure, atomic substitution [52,53], metal doping [53–58], chemical [47], and the application of an electric field [59,60] operations. The use of external hydrostatic pressure is one of the existing techniques that are quick and effective for changing the energy gap of perovskites [61–67], which alters the materials' optical and electronic properties. Perovskite materials could be acceptable for use in solar and optoelectronic applications by altering their properties [44,51,64]. Additionally, it has been found that harnessing hydrostatic pressure to change the energy gap from the indirect band to the direct band is advantageous in several cubic perovskites [45,52,66,68–71]. The materials in the indirect band gap might produce phonons that would have the effect of heating the optoelectronic devices and reducing their efficiency [49,72–74]. The energy band gap of the non-toxic halide cubic perovskite CsBX$_3$ (B=Sn, Ge; X = Cl, Br) was brought down to 0 eV by applying hydrostatic pressure, changing the materials' nature from semiconductor to conductor [50]. The non-toxic cubic halide perovskites ACaX$_3$ (A = Cs, Rb, K, Na; X = I, Br, Cl, F) have undergone first-principles calculation and shown reliable results [74–78]. These Ca-based cubic not-toxic halide perovskites have a large band gap and could be used in the production of transparent optical coatings and lens materials [79,80]. Some of the Ca-based cubic non-toxic perovskites, including KCaX$_3$ (X = F, Cl) [30,31], and ACaF$_3$ (A = Rb, Cs), have previously been subjected to hydrostatic pressure. By increasing hydrostatic pressure of up to 14 GPa for KCaF$_3$ and RbCaF$_3$, respectively, the energy band gap of each material was converted from an indirect band to a direct band [75,81, 82]. Additionally, under elevated hydrostatic pressure, ACaF$_3$ (A = K, Rb, Cs) showed better mechanical qualities [75,82,83]. The theoretical examination of CsCaCl$_3$, RbCaCl$_3$, and KCaCl$_3$ among the aforementioned Ca and Cl-based non-toxic halide perovskites have been carried out at room temperature, and it discloses an indirect energy band gap [27,75,77]. On the other hand, Fr-based compounds, such as FrSnCl$_3$, and FrGeCl$_3$ showed direct nature in the band gap [84].

Strontium (Sr^{2+}) and Calcium (Ca^{2+})-based inorganic perovskites have emerged as promising alternatives to Lead (Pb^{2+}) perovskites due to their enhanced optical conductivity and absorption properties. Francium (Fr)-based halide perovskites also exhibit high conductivity and absorptivity in the lower energy range, presenting theoretical advantages over toxic Pb-based counterparts. Francium, being the heaviest and most electropositive alkali metal, introduces unique electronic and structural characteristics that could lead to novel optoelectronic behaviors and offer new insights into perovskite compounds. Investigating Fr-based perovskites expands the frontier of material science, enhancing our understanding of heavy element incorporation in perovskite structures. Consequently, this study focuses on the perovskite compound FrCaCl$_3$.

Nazmul Hasan et al. have explored the structural, electronic, optical, and mechanical properties of Pb-free Fr-based cubic perovskite materials FrBX$_3$ (B=Ge, Sn; X = Cl, Br, I) [84]. However, the behavior of the FrCaCl$_3$ halide perovskite under both pressurized and non-pressurized conditions remains unexamined. There is a gap in research concerning how FrCaCl$_3$ halide perovskite behaves when subjected to pressure, as well as its characteristics in non-pressurized conditions. In this regard, this DFT-based computational study evaluates the structural, electronic, bonding, anisotropic elastic, mechanical, and optical attributes of the FrCaCl$_3$ compound both with and without hydrostatic pressure.

2. Computational and geometry optimization details

The first-principles calculations are performed using the Cambridge Serial Total Energy Package (CASTEP) [85] code in Materials Studio version 8.0, an application of the plane-wave pseudo-potential total energy technique established on density functional theory (DFT). The exchange-correlation effect was handled using the generalized gradient approximation (GGA) proposed by Perdew-Burke-Ernzerhof (PBE) [86]. The interaction of valence electrons with ion cores is simulated using the Vanderbilt-type ultrasoft pseudopotentials [87]. To calculate all the physical parameters, the plane-wave basis set cut-off is fixed to 900 eV. The Monkhorst-Pack [88] approach with a $12 \times 12 \times 12$ special k-point mesh is implemented to add unique positions sampling throughout the Brillouin zone. To quickly find the structure with the minimum energy, the Broyden-Fletcher-Goldfarb-Shanno (BFGS) minimizing approach [89] is also used in geometry optimization. The convergence factors are defined to be an overall energy difference with less than 5×10^{-6} eV/atom, a maximum ionic Hellmann-Feynman force of less than 0.01 eV, a maximum displacement that is less than 5×10^{-4} Å, and maximum stress compared with fewer than 0.02 GPa. The geometrically relaxed structure is used to determine all the
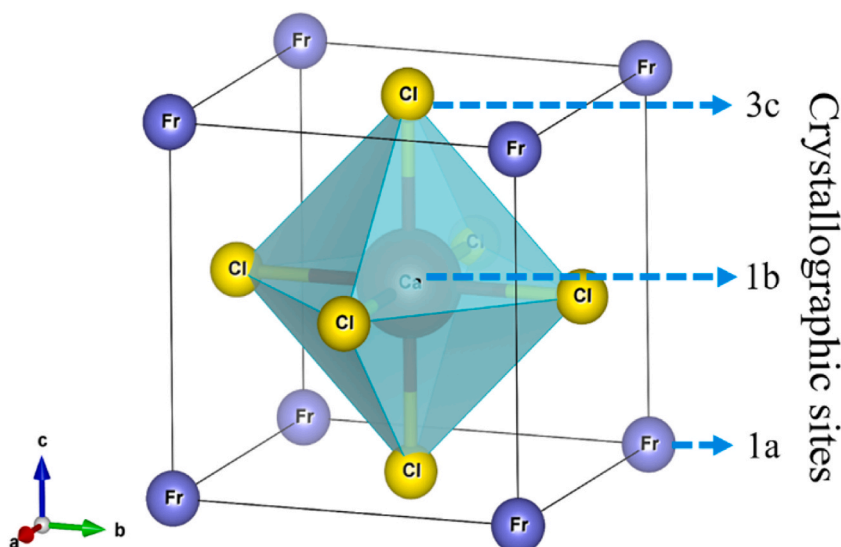
Fig. 1. Crystal structure of FrCaCl$_3$.

necessary physical characteristics. A pressure gradient up to 150 GPa with intervals of 30 GPa is used in this investigation. The three-dimensional (3D) optimized crystalline structure is depicted using the VESTA software [90]. The ELATE tool is used to generate anisotropic curves of Young's modulus, shear modulus, and Poisson's ratio in two-dimensional (2D) and three-dimensional (3D) directions [91,92]. The elastic stiffness constants of inorganic cubic FrCaCl$_3$ halide perovskite were calculated using the finite stress-strain method [1,22,69].

Electronic structure calculations were conducted using the GGA-PBE model with density mixing. Additionally, to improve the accuracy of these calculations, the hybrid HSE06 functional was employed, employing an All bands/EDFT electronic minimizer approach. The hybrid HSE06 electronic exchange correlation functional offers notable advantages in electronic band structure calculations. Unlike traditional density functionals, HSE06 incorporates a fraction of exact exchange, providing a more accurate description of electronic interactions, particularly for systems with substantial electron correlation. This leads to improved predictions of band gaps and electronic properties, addressing the well-known issue of underestimation common in standard functionals. The inclusion of non-local exchange terms enhances the treatment of long-range interactions, making HSE06 particularly valuable for accurately modeling materials with diverse bonding characteristics.

3. Results and discussion

3.1. Structural properties and phase stability

The Fr-based non-toxic halide perovskite FrCaCl$_3$ belongs to a cubic crystal system and is a member of the $Pm\overline{3}m$ (#221) space group [84]. In Fig. 1, the optimized crystalline structure of FrCaCl$_3$ is illustrated with crystallographic positions. The unit cell structure of the FrCaCl$_3$ compound comprises five atoms and one formula unit. The radioactive Fr atom inhibits the corner at 1a Wyckoff site (0, 0, 0), the Ca atom takes place in the body-centered position at 1b Wyckoff site (0.5, 0.5, 0.5), and the Cl atom fills the face-centered site at 3c Wyckoff site (0, 0.5, 0.5).

Before embarking on the computational analysis of other characteristics, it is imperative to assess the stability of FrCaCl$_3$, as experimental synthesis remains unrealized. Insights into cubic stability are derived through calculations involving the Goldschmidt tolerance factor (t) and octahedral factor (m). The determination of these stability measures employs the formulas [57,64,70,80,84]:

$$t = \frac{(R_{Fr} + R_{Cl})}{\sqrt{2(R_{Ca} + R_{Cl})}}, \text{ and}$$

$$m = \frac{R_{Ca}}{R_{Cl}}.$$

where, R_{Fr}, R_{Ca}, and R_{Cl} are ionic radius of Fr$^+$ (1.80 Å), Ca^{2+} (0.99 Å) and Cl$^-$ (1.81 Å), respectively. The calculated Goldschmidt tolerance factor and octahedral factor for FrCaCl$_3$ are 0.912 and 0.547, respectively. For cubic stability, a compound should exhibit a tolerance factor within the range of 0.81–1.00 [70] and an octahedral factor between 0.37 and 0.859.

Abeeha Batool et al. calculated the Goldschmidt tolerance factor (t) by the following relation [66]:

Table 1
Bond lengths (L), and Goldschmidt tolerance factor (t) of FrCaCl$_3$ under various hydrostatic pressure.

Pressure (GPa)	Bond length, L (Å)		Tolerance factor, t
	L$_{Fr-Cl}$	L$_{Ca-Cl}$	
0	3.617	2.558	0.999
30	3.266	2.310	0.999
60	3.113	2.201	0.999
90	3.013	2.131	0.999
120	2.938	2.077	1.000
150	2.878	2.035	0.999

Table 2
The simulated theoretical values of lattice parameters and formation energy under hydrostatic pressure.

| Compound	Pressure (GPa)	Lattice constant, a (Å)		Volume, V (Å^3)		Formation energy, E$_f$ (eV/atom)	Remarks
		GGA	HSE06	GGA	HSE06		
FrCaCl$_3$	0	5.487	5.116	165.17	133.88	−5.816	This work
KCaCl$_3$	0	5.397	–	157.20	–	–	[27]
FrGeCl$_3$	0	5.37	–	–	–	–	[84]
FrSnCl$_3$	0	5.64	–	–	–	–	[84]
CsCaCl$_3$	0	5.47	–	–	–	–	[77]
FrCaCl$_3$	30	4.740	4.619	106.53	98.56	−4.897	This work
FrCaCl$_3$	60	4.478	4.402	89.80	85.32	−3.959	This work
FrCaCl$_3$	90	4.320	4.261	80.59	77.38	−3.088	This work
FrCaCl$_3$	120	4.203	4.155	74.27	71.76	−2.242	This work
KCaCl$_3$	120	4.101	–	69.00	–	–	[27]
FrCaCl$_3$	150	4.111	4.070	69.49	67.44	−1.411	This work
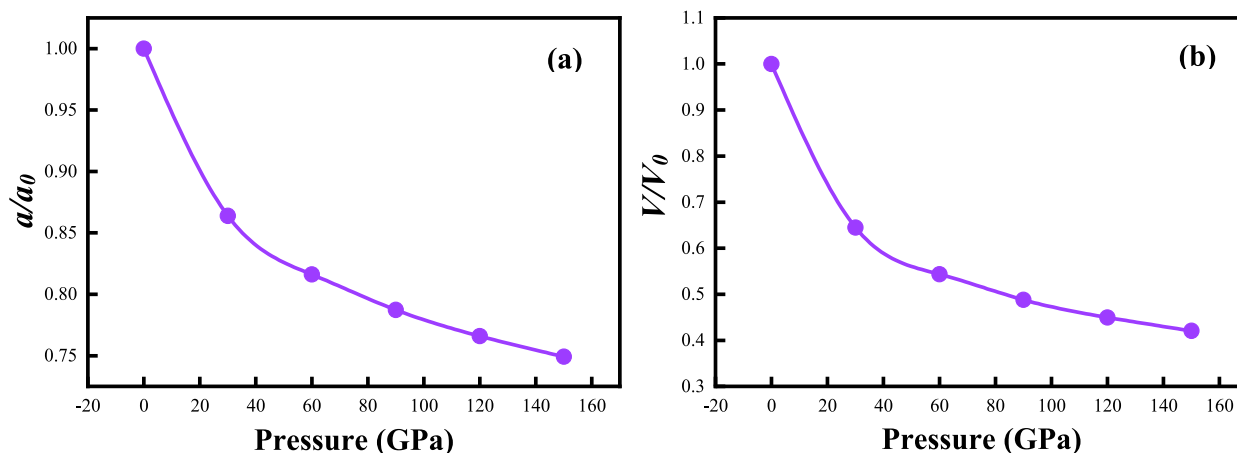
Fig. 2. (a) Lattice constant vs. pressure, and **(b)** lattice volume vs. pressure.

$$t = \frac{0.707(L_{Fr-Cl})}{L_{Ca-Cl}}.$$

The equation provided defines L$_{Fr-Cl}$ as the bond length between Fr and Cl, and L$_{Ca-Cl}$ as the bond length between Ca and Cl. Table 1 showcases the computed bond lengths L$_{Fr-Cl}$ and L$_{Ca-Cl}$, along with the Goldschmidt tolerance factor (t), under various pressure conditions. In Tables 1, it is evident that the Fr−Cl bond surpasses the length of the Ca–Cl bond, a result of the notable electronegativity difference between the respective elements. This finding correlates with the estimations of ionic and covalent interactions in Fr−Cl and Ca–Cl, respectively, as confirmed by the charge density mapping of FrCaCl$_3$ (Fig. 7). As pressure intensifies, the bond lengths for both substances consistently decrease as the atoms in the compound are forced closer together, reaching their minimal lengths at 150 GPa. This implies that heightened pressure facilitates the formation of stronger bonds characterized by reduced bond lengths. As per Batool et al., in the context of an ideal cubic structure, the tolerance factor should fall within the range of 0.93–1.02 [66]. A scrutiny of Table 1 reveals that FrCaCl$_3$ aligns with these criteria, suggesting its adherence to cubic stability.

Table 2 contains the computed data of the pressure-dependent lattice parameter and unit cell volume for the FrCaCl$_3$ cubic perovskite using both the GGA and hybrid HSE06 approximation functional. The findings suggest that employing the HSE06 functional
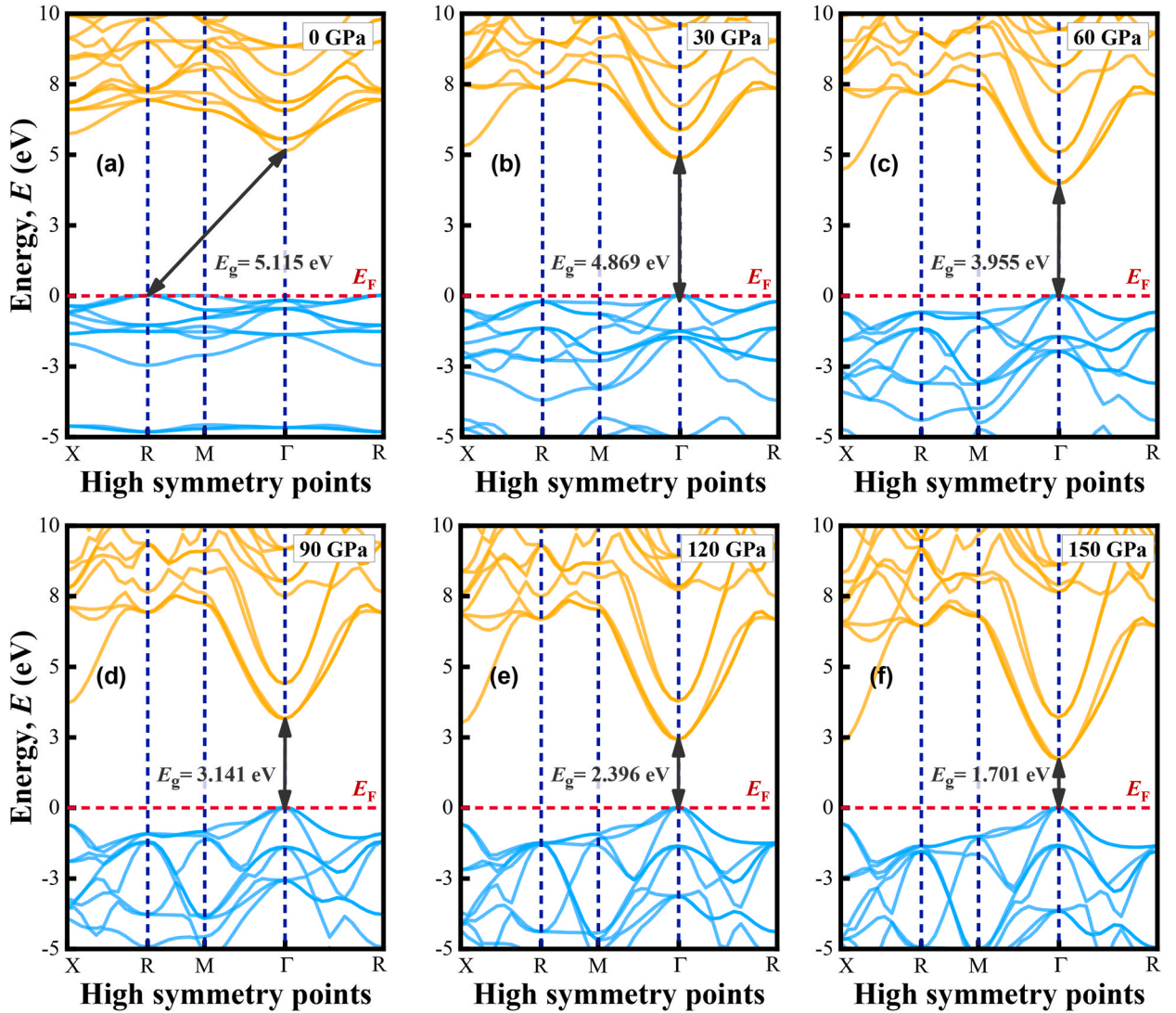
Fig. 3. The effect of applied pressure at **(a)** 0 GPa, **(b)** 30 GPa, **(c)** 60 GPa, **(d)** 90 GPa, **(e)** 120 GPa, and **(f)** 150 GPa on the band structures of FrCaCl$_3$.

results in slightly diminished lattice parameters in comparison to the GGA functional, both under pressure and in the absence of it. The subtle discrepancies observed in the calculations stem from the reliability inherent in the hybrid HSE06 exchange correlation potential. Nevertheless, the lattice parameters determined through the HSE06 method demonstrate a consistent trend akin to those obtained from the GGA-PBE scheme, irrespective of the presence or absence of hydrostatic pressure. When subjected to hydrostatic pressure, the lattice parameters undergo a reduction. This phenomenon can be attributed to the external pressure compelling the atoms beyond their repulsive forces, causing them to occupy a more confined space.

In this study, the optimized lattice constant value of the non-toxic FrCaCl$_3$ compound exhibits a similar trend when compared to KCaCl$_3$ (5.397 Å) [27], CsCaCl$_3$ (5.47 Å) [77], FrGeCl$_3$ (5.37 Å), and FrSnCl$_3$ (5.64 Å) [84] compounds. Fr and Cs atoms belong to the same periodic group, and both compounds have CaCl$_3$ in their structure, that is why both FrCaCl$_3$ (5.487 Å) and CsCaCl$_3$ compounds have closer values of lattice constant. Both the lattice constant and the unit cell volume responses to applied hydrostatic pressure (0–150 GPa) are illustrated in Fig. 2(a) (lattice constant vs. pressure) and Fig. 2(b) (lattice volume vs. pressure), respectively. As the pressure rises, it is observed that the lattice constant, along with the cell volume, is decreasing. At a pressure of 120 GPa, the lattice constants of FrCaCl$_3$ and KCaCl$_3$ exhibit closely aligned values [27].

Furthermore, structural stability was assessed through the calculation of the formation energy (E$_f$). The determination of this parameter relies on the equation outlined in previous works [57,64,66]:

$$E_f \ (FrCaCl_3) = \frac{[E_{total}(FrCaCl_3) - E_s(Fr) - E_s(Ca) - 3E_s(Cl)]}{N}.$$

Table 3
The calculated values of energy band gap (E_g) of cubic $FrCaCl_3$ under applied pressure.

Pressure (GPa)	Band gap, E_g (eV)		Nature
	GGA	HSE06	
0	5.115	5.705	Indirect
30	4.869	5.923	Direct
60	3.955	4.964	Direct
90	3.141	4.134	Direct
120	2.396	3.322	Direct
150	1.701	2.618	Direct
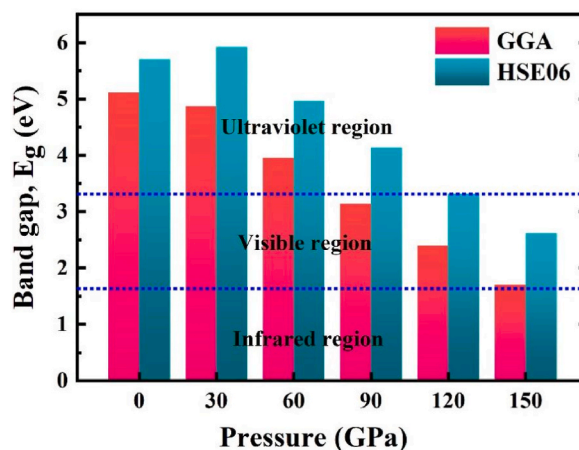
Fig. 4. The decreasing tendency of band gap of $FrCaCl_3$ perovskite under pressure.

In the context of the $FrCaCl_3$ unit cell structure, the energies of Fr, Ca, and Cl atoms are denoted as $E_s(Fr)$, $E_s(Ca)$, and $E_s(Cl)$, respectively. The overall energy of the unit cell, represented as $E_{total}(FrCaCl_3)$, considers the total number of atoms (N) within the unit cell. The formation energy values calculated through the HSE06 approximation functional for $FrCaCl_3$ under varying pressure conditions are tabulated in Table 2. The consistent negativity of the formation energy (E_f) across all pressure conditions establishes the thermodynamic stability of this inorganic halide perovskite system.

3.2. Electronic properties

The investigation of the electronic properties of a material, especially the band structure and density of states (DOS), may be crucial in acquiring complete knowledge of its optical characteristics. Fig. 3 represents the band structure of the $FrCaCl_3$ compound under varying hydrostatic pressure determined by using GGA-PBE functional. Furthermore, for enhanced accuracy in determining electronic structures, the hybrid HSE06 electronic exchange correlation (XC) functional is utilized. Table 3 provides the electronic energy band gap values obtained through both the GGA and hybrid HSE06 methods. Notably, the application of the HSE06 method results in enhanced band gap values for the $FrCaCl_3$ perovskite.

The band structure is diversified from -5 to $+10$ eV where the red horizontal dashed line at 0 eV stipulates the Fermi level (E_F) and there also the colored lines below and above the E_F represent the valence band (VB) and conduction band (CB), respectively. The perceived band gap (E_g) at zero pressure is 5.115 eV having the nature of an indirect band gap since the valence band maxima (VBM) are situated at the R point and the conduction band minima (CBM) are placed at the Γ point. Previous work based on cubic $FrBX_3$ (B=Ge, Sn; X = Cl, Br, I) perovskite compounds have been done by Nazmul and associates have found most of the Fr-based halide structures exhibit semiconducting behavior as well as direct nature in the band gap [84]. Additionally, Nayak and associates discovered that the implemented functional had little impact on the band structure's general behavior or the fluctuation of E_g under pressure; as a result, the PBE approach can deliver outcomes that are largely accurate [62,93]. This means that the GGA-PBE functional ought to be employed for pressure experiments on materials. At zero applied pressure, both $FrCaCl_3$ and $CsCaCl_3$ compounds exhibit an indirect band gap nature, along with similarities in the band gap values: $FrCaCl_3$ (5.115 eV) and $CsCaCl_3$ (5.35 eV) [77], respectively.

By employing the hybrid HSE06 XC functional, the indirect band gap is estimated as 5.705 eV at zero GPa. It can be observed from Table 3 that, with increasing hydrostatic pressure, the band gap between the valence band (VB) and conduction band (CB) is decreasing for both the GGA and hybrid HSE06 methods. The decrease in the band gap of $FrCaCl_3$ under extreme hydrostatic pressure can be attributed to the compression of its crystal lattice. As pressure increases, the atoms in the perovskite structure are forced closer together, reducing the interatomic distances. This compression alters the electronic band structure of the material, potentially shifting
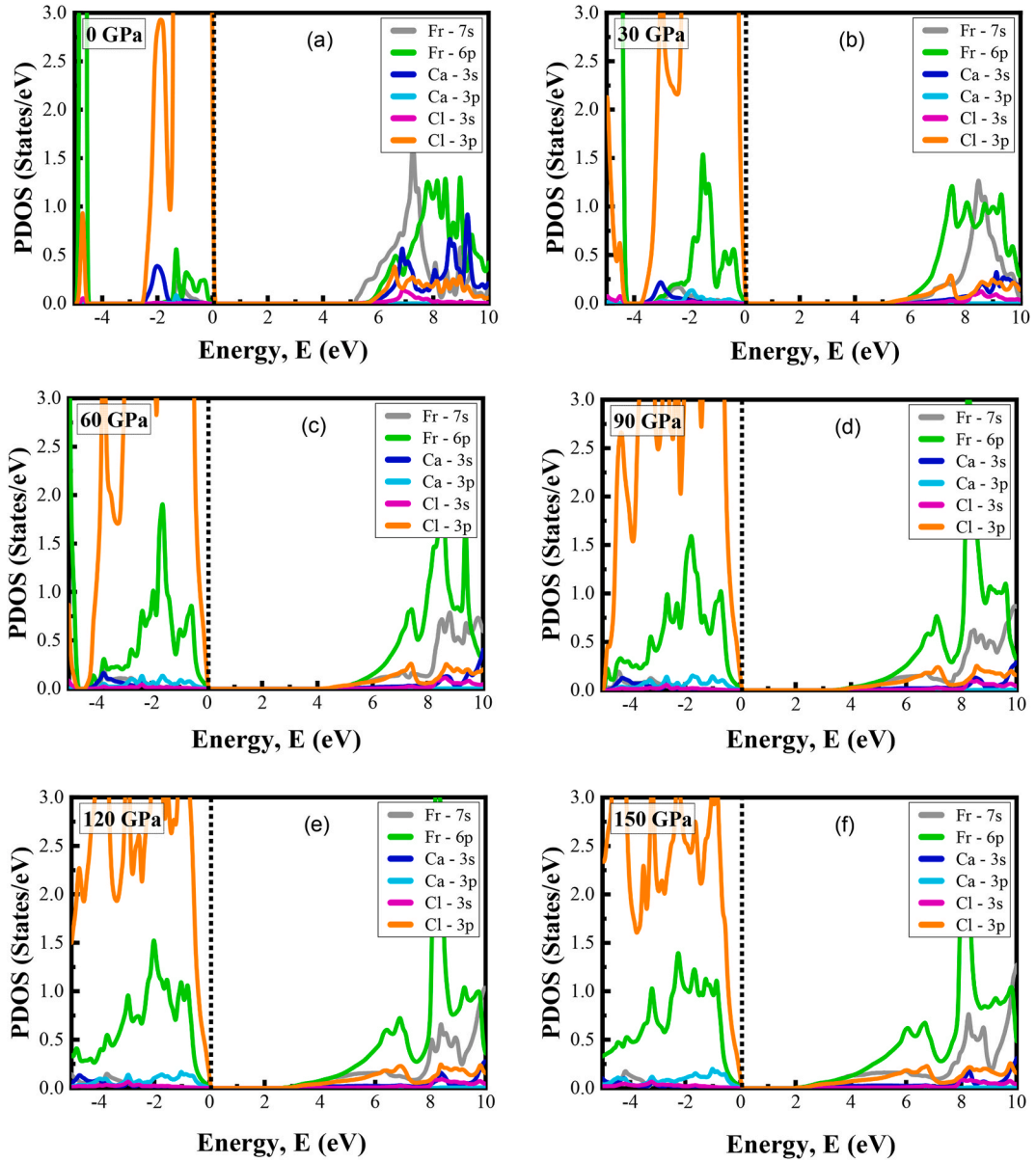
Fig. 5. The partial density of states (PDOS) of FrCaCl$_3$ perovskite at **(a)** 0 GPa, **(b)** 30 GPa, **(c)** 60 GPa, **(d)** 90 GPa, **(e)** 120 GPa, and **(f)** 150 GPa pressure.

the positions of the valence and conduction bands and affecting the band gap energy.

At zero pressure, an indirect band gap was observed between R and Γ points. However, with increasing pressure the valence band maxima (VBM) moved from R point to Γ point, making it a direct band gap nature evident at 30 GPa (Fig. 3). The externally applied pressure lengthens the valence band, causing it to extend linearly to higher energies in the region. Such energy shifts cause specific state rearrangement and tend to result in an indirect band gap to a direct band gap transformation [28].

Under increasing pressure, the indirect to direct shifting of the band gap was also discerned for cubic halide perovskites such as KCaCl$_3$ (4.76 eV), and RbCaCl$_3$ (6.39 eV) [70,76,82]. This transition may lower the energy required for electrons to shift from VB to CB, thereby enhancing the performance of solar devices [73,94]. The indirect to direct band gap transition is also observed in the case of Cl-based perovskite compounds which is evident in KSrCl$_3$ (4.45eV) [95]. Fr-based perovskite has semiconducting nature noticeable in the work of Nazmul and associates [84]. Eventually, the band gap is adjustable as a consequence of pressure, shifting from the ultraviolet area to the visible light range, as indicated in Table 3 and Fig. 4.

The investigation of the partial density of states (PDOS) is crucial for gaining a deeper understanding of the electronic band structure. The PDOS of FrCaCl$_3$ perovskite at different hydrostatic pressures is shown in Fig. 5, where the black perpendicular dashed line at 0 eV is the E$_F$. The VB of non-pressurized states is dominated by Fr-6p, Cl-3p, and Ca-3s, with Ca-3p states contributing very
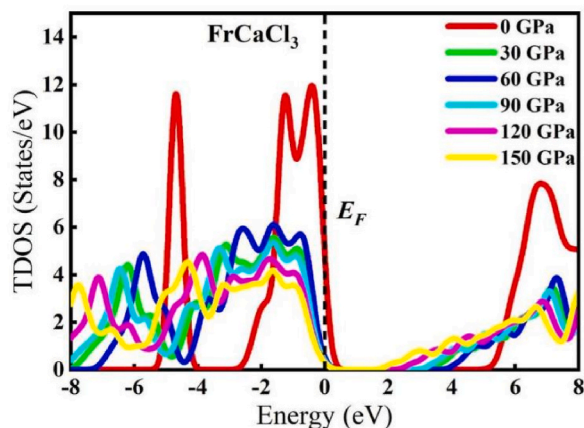
Fig. 6. The total density of states (TDOS) of FrCaCl$_3$ perovskite under various pressure.
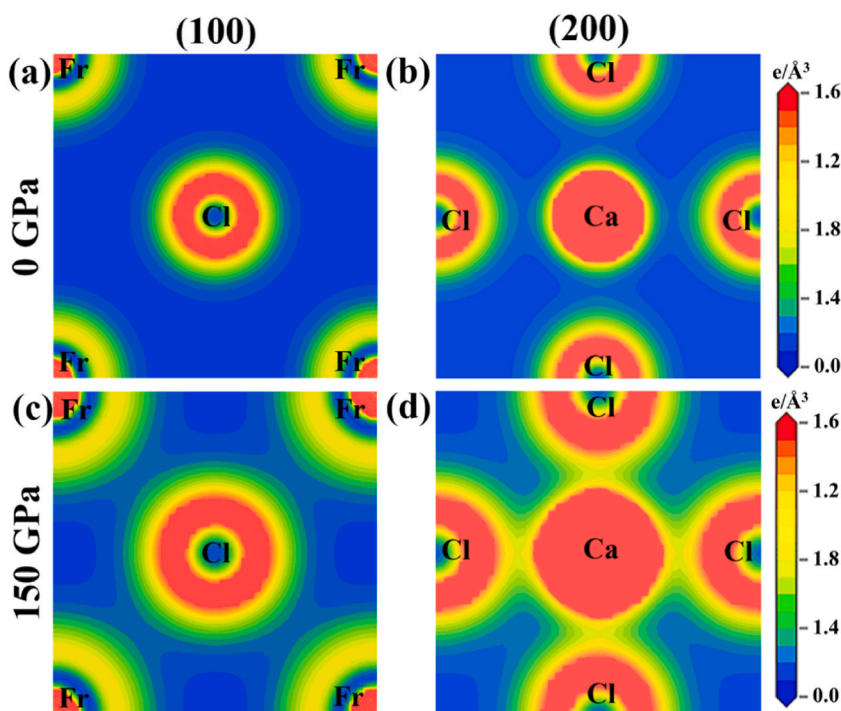

Fig. 7. The charge density map of cubic perovskite FrCaCl$_3$ along the (100) and (200) crystallographic plane at (**a, b**) 0 GPa pressure, and (**c, d**) 150 GPa pressure.

little. However, increasing the applied pressure reduces the contribution of Fr-6p and Ca-3s states while increasing the contribution of Cl-3p and Ca-3p states. Apart from that, the CB mainly originated from the contribution of Fr-7s, Fr-6p, Ca-3s, Cl-3p, and Cl-3s states at zero pressure. The contribution of Ca-3s and Cl-3s states reduces with increasing pressure. Additionally, the band gap is narrowed in case of high pressure due to the involvement of Fr-6p, Fr-7s, and Cl-3p states. Fig. 6 illustrates the total density of states (TDOS) for FrCaCl$_3$ perovskite under various hydrostatic pressures. The TDOS curves clearly demonstrate the narrowing of the band gap as pressure increases.

To comprehend the behavior of bonding between cation and anion atoms in FrCaCl$_3$, the electron charge density map is examined. Red hues indicate the maximum charge level, while blue colors indicate the lowest charge presence. In FrCaCl$_3$, the bonding between Fr and Cl is represented by the (100) plane. Fr–Cl has a weak ionic bond at zero GPa pressure (Fig. 7(a)), however, it grows stronger when maximum pressure (150 GPa) is applied (Fig. 7(c)). The lattice plane (200) exhibits an ionic bonding of Ca–Cl at zero pressure (Fig. 7(b)) which strengthened with an increase in pressure and began to exhibit overlapping covalent character as shown in Fig. 7(d). The smaller atomic distances caused by the external pressure may be the key factor for the greater electron density between the FrCaCl$_3$
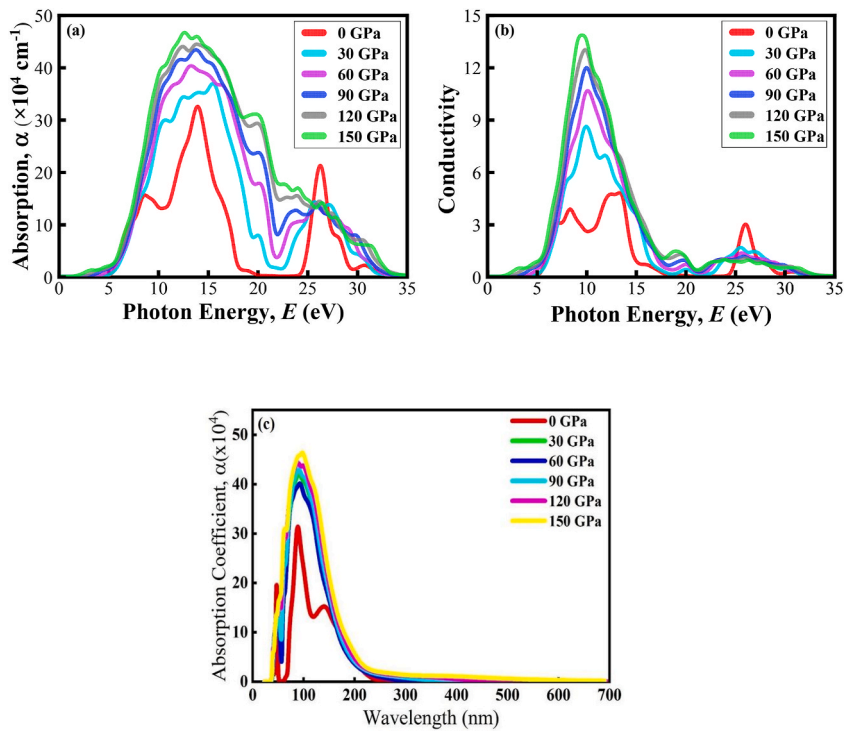
Fig. 8. The pressure-induced **(a)** absorption, and **(b)** conductivity with respect to photon energy, and **(c)** absorption with respect to photon wavelength of FrCaCl$_3$.
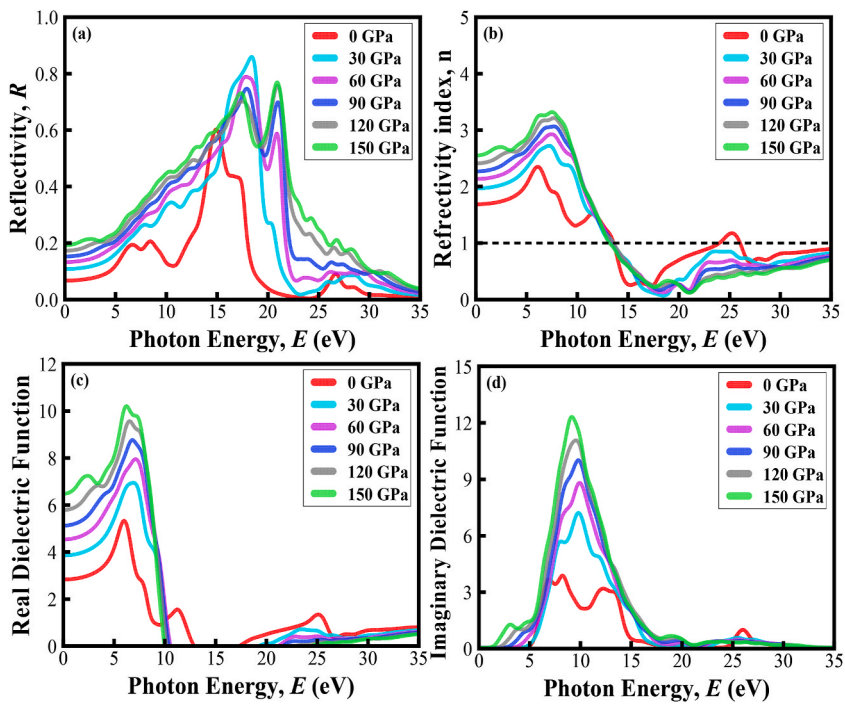

Fig. 9. The pressure-induced **(a)** Reflectivity, **(b)** Refractive index, **(c)** Real part of dielectric function, and **(d)** Imaginary part of dielectric function of FrCaCl$_3$.

atoms.

3.3. Optical properties

Understanding optical properties are crucial for forecasting material performance in applications involving optoelectronic devices [96–98]. Materials' optical properties lead to their viability and usefulness from a commercial standpoint, particularly in photonic devices. Under various hydrostatic pressures starting from zero GPa to 150 GPa, the optical absorption, conductivity, reflectivity, refractive index, and dielectric function of $FrCaCl_3$ are evaluated. Because of its wide-ranging band gap (5.705 eV) in the ultra-violet (UV) region, the cubic halide perovskite $FrCaCl_3$ is unsuitable for solar cell applications. As a result, further research is needed to ameliorate the efficiency of photovoltaic cells and optoelectronic applications. Using pressure to lower the band gap of Fr-based halide perovskite can be an effective strategy [73,82,94,99–102].

The shrinkage in the band gap of the electronic band structure under extreme hydrostatic pressure (Fig. 3) is discernible from the ultraviolet (UV) to the visible light range. This observed phenomenon suggests the potential utility of the compound in the realm of photocatalytic materials and optoelectronic devices operating within the visible spectrum. This material is better suited for usage in optoelectronic applications as the band gap character changes from indirect to direct at a hydrostatic pressure of 30 GPa.

The absorption coefficient is one of the optical properties used to measure the efficiency of solar cells [74]. The ability of a material to soak up light energy offers critical knowledge about the effectiveness of solar energy conversion when exposed to visible light [1]. Fig. 8(a-b) and Fig. 9(a-d) depicts an insightful analysis of several optical properties for the non-toxic $FrCaCl_3$ cubic halide perovskite determined for energy ranges up to 35 eV at various pressures of (0, 30, 60, 90, 120, and 150) GPa. It is evident that as pressure increases, so does the amount of absorptions in the ultraviolet energy range showing a similar trend in every pressure condition. Despite being physically anisotropic, $FrCaCl_3$ exhibits optically isotropic behavior in the lower energy region at zero pressure, which is the major criterion for scintillator applications [103,104,96]. As the pressure increases, the highest peaks of absorption (α) in different pressure lean towards higher energy regions. At 150 GPa pressure, the greatest optical absorption coefficient peak is evident at ~14 eV light energy similar to $FrGeCl_3$ and $FrSnCl_3$ compounds [105]. Fig. 8(a) also shows the widest absorption peak is in the ultraviolet region, which suggests that $FrCaCl_3$ can be an effective material for photocatalytic activity. Additionally, to highlight the lower energy range, Fig. 8(c) displays the optical absorption plot based on the photon wavelength range of 0–700 nm.

Another key metric that identifies a material's electrostatic response is optical conductivity (σ). Fig. 8(b) illustrates the visual depiction of optical conductivity as a consequence of photonic energy. Photoconductivity is the measurement of how many photons travel throughout the material and can be calculated using optical conductivity [106]. It is also evident that as pressure increases, optical conductivity in the ultraviolet energy range also increases, showing a similar trend in every pressure condition. At zero GPa pressure, the highest amount of conductivity for $FrCaCl_3$ is evident at 13.9 eV. On the other hand, at 150 GPa pressure, the greatest optical conductivity peak is seen at ~9.5 eV light energy. As materials absorb photon energy and release free carriers, conductivity, as well as absorption spectra follow a similar trend. However, neither α nor σ begins at 0 eV for the material under hydrostatic pressure ranging from 0 to 150 GPa, validating the semiconducting nature of the $FrCaCl_3$ compound. This increased conductivity indicates that $FrCaCl_3$ will be an efficient material under pressure, resulting in more efficient optoelectronic devices.

A material's optical reflectivity (R) can be utilized to determine the characteristics of its surface, and it specifies how much light the surface of a material can reflect [107]. Fig. 9(a) displays the reflectivity vs. photon energy of the $FrCaCl_3$ compound under pressure. When pressure is applied, the number of R escalates, which can lower the performance of the photovoltaic system. At zero GPa, the overall reflectivity value at zero frequency, R(0) is 6.2 % of the total radiation, computed for $FrCaCl_3$. As the amount of reflectivity is much lower than 10 %, $FrCaCl_3$ can be considered a highly transparent material in the case of the infrared radiation (IR) region as well as the visible region. For that reason, it has the potential to serve as transparent coatings and excellent lens material. When the pressure is increased to 150 GPa, the reflectivity is observed at zero frequency, constituting 18.9 % of the overall radiation. It is also evident that the material reflects more than 85 % of light at approximately 18.5 eV. Therefore, more research is needed to find ways to lower reflectivity in low-energy areas, which could enhance absorption and solar cell performance. It's important to note that the increased value of R under hydrostatic pressure in UV regions indicates that the material could be a potential candidate for reducing solar heat.

An elemental characteristic that describes how a material affects the speed of light passing through it is the refractive index (n) [108]. It also provides information of material to estimate its usefulness for practical device applications [109]. The n has a declining trend and reaches its peak in the UV energy range, where it is relatively constant at zero GPa, as shown in Fig. 9(b). At zero pressure the static value of the refractive index is n(0) = 1.68, which increases with increase in hydrostatic pressure. $FrCaCl_3$ is highly suitable for usage in solar cells, QLED, OLED [110] and waveguides as the n(0) starts to increase with an increase in hydrostatic pressure.

The dielectric function is the key factor that influences a material's charge-carrier recombination rate [111]. It is expressed as $\varepsilon(\omega) = \varepsilon_1(\omega) + i\varepsilon_2(\omega)$, where the real and imaginary portions of the dielectric function are denoted by $\varepsilon_1(\omega)$ and $\varepsilon_2(\omega)$, respectively. The real component indicates polarization inside the material, whereas the imaginary part reflects energy dissipation. Photovoltaic cells with higher static dielectric constants experience lower recombination rates [112]. As a result, the amount of the dielectric function in relation to the incident photon energy determines a material's suitability for use in optoelectronic devices in a very significant way [113,114]. Fig. 9(c) and (d) depict the changes in the real and imaginary components of the dielectric constant with and without hydrostatic pressure. According to Fig. 9(c), applying pressure results in a greater static dielectric function $\varepsilon_1(\omega)$ than in a non-pressurized system, which could improve the device's efficiency. The lower energy gap of the crystal system under hydrostatic pressure shows the increasing values of $\varepsilon_1(\omega)$ which further produces higher $\varepsilon_1(\omega)$ for the compound $FrCaCl_3$ in the visible spectrum. The value of ε_1 drops below zero showing negativity around 13 eV for every pressure condition, and only zero pressure curve shows a glimpse of positive value around 24 eV after the drop. The imaginary part of the dielectric function is significantly appertained to the

Table 4

The calculated elastic constants C_{ij} (GPa) values of FrCaCl$_3$ at numerous hydrostatic pressures.

Compound	Pressure (GPa)	C_{11}	C_{12}	C_{44}	Remarks
FrCaCl$_3$	0	49.78	11.31	10.84	This work
KCaCl$_3$	0	54.06	9.26	7.80	[27]
CsCaCl$_3$	0	56.91	9.69	10.23	[77]
FrGeCl$_3$	0	52.41	13.69	12.17	[84]
FrSnCl$_3$	0	48.41	9.82	6.54	[84]
FrCaCl$_3$	30	276.43	66.68	25.39	This work
FrCaCl$_3$	60	467.25	117.35	36.89	This work
FrCaCl$_3$	90	642.23	166.32	47.13	This work
FrCaCl$_3$	120	805.54	214.15	56.45	This work
KCaCl$_3$	120	818.07	170.96	6.82	[27]
FrCaCl$_3$	150	985.39	261.13	65.03	This work

Table 5

The computed elastic anisotropy (A), Poisson's ratio (ν), Pugh's ratio (B/G), shear modulus (G) in GPa, Young's modulus (E) in GPa, and bulk modulus (B) in GPa of FrCaCl$_3$ at different applied pressures.

Compound	Pressure (GPa)	B	G	E	ν	B/G	A	Remarks
FrCaCl$_3$	0	24.13	13.67	34.49	0.262	1.77	0.564	This work
KCaCl$_3$	0	24.20	12.10	31.11	0.285	2.00	0.35	[27]
CsCaCl$_3$	0	25.430	14.406	36.35	0.363	1.765	0.433	[77]
FrGeCl$_3$	0	26.60	14.67	37.18	0.27	1.81	–	[84]
FrSnCl$_3$	0	22.68	10.27	26.77	0.30	2.21	–	[84]
FrCaCl$_3$	30	136.60	46.81	126.02	0.346	2.92	0.242	This work
FrCaCl$_3$	60	233.99	73.01	198.39	0.359	3.20	0.211	This work
FrCaCl$_3$	90	324.96	96.42	263.22	0.365	3.37	0.198	This work
FrCaCl$_3$	120	411.28	117.80	322.61	0.369	3.49	0.191	This work
KCaCl$_3$	120	386.66	72.36	204.33	0.411	5.34	0.02	[27]
FrCaCl$_3$	150	493.54	137.43	377.28	0.372	3.59	0.180	This work

material band structure, density of states, and absorption coefficient [115]. The absorption spectra shown in Fig. 8(a) is ultimately justified by the fact that the peak of $\varepsilon_2(\omega)$ rises as pressure rises (Fig. 9(d)). With an increase in photon energy, the $\varepsilon_2(\omega)$ falls from a peak value and eventually reaches zero. The possible use of FrCaCl$_3$ in integrated circuits and microelectronics is demonstrated by the increased $\varepsilon_2(\omega)$ in the low-frequency band.

3.4. Mechanical properties

Elastic constants (C_{ij}) are the most essential variables to consider when examining the mechanical characteristics of solid materials [116,117]. They are crucial in defining a variety of material characteristics, such as brittleness, ductility, stiffness, anisotropy, and so on [1,73,74,118]. It is also possible to infer a material's mechanical stability from C_{ij} [3,64]. The mechanical properties are determined using the 'finite strain' theory [119]. It is essential to acknowledge how pressure affects the C_{ij} because the lattice constant of FrCaCl$_3$ reduces with applied pressure as shown in Fig. 2. Three distinct elastic constants, C_{11}, C_{12}, and C_{44}, representing the elastic modulus tensor, are observed in the FrCaCl$_3$ cubic perovskite. Table 4 shows the computed C_{ij} at numerous applied pressures with the available reported theoretical results. It is observed that the values of C_{ij} are simultaneously increased under applied pressure. The calculated C_{ij} at zero pressure is well suited to the results of the earlier study of Ca and Cl-based perovskite compounds [1,120].

The renowned Born stability criteria are what determine the cubic crystals' mechanical stability [121]:

$C_{11} > 0$, $C_{44} > 0$, $(C_{11}–C_{12}) > 0$, and $(C_{11}+2C_{12}) > 0$

From Table 4 it is noticeable that the derived elastic constants successfully meet the Born stability requirements. It is clear that FrCaCl$_3$ is mechanically stable both with and without external pressure.

The Voigt-Reuss-Hill (VRH) method is commonly employed for estimating the bulk modulus (B), shear modulus (G), and Young's modulus (Y). Utilizing the following specific formulas, these moduli can be calculated as part of the analysis process [97,98,122,123].

$$\text{Bulk modulus}, B = \frac{1}{3}(C_{11} + 2C_{12})$$

$$\text{Shear modulus}, G = \frac{1}{5}(3C_{44} + C_{11} - C_{12})$$
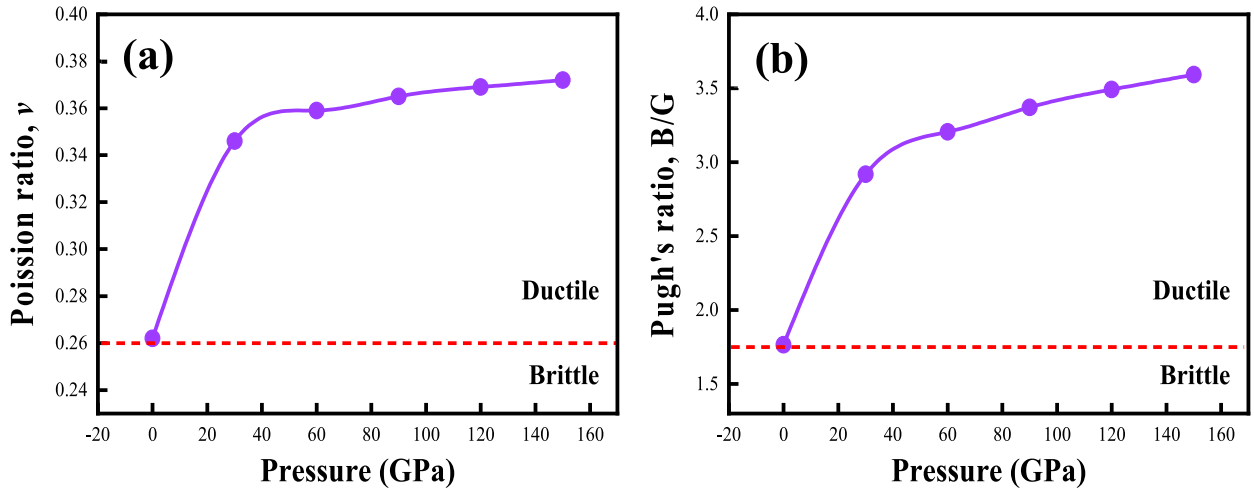
$$\text{Young's modulus}, E = \frac{9BG}{3B + G}$$

Fig. 10. Variations in **(a)** Poisson's ratio, and **(b)** Pugh's ratio of $FrCaCl_3$ under pressure.

Table 5 shows the computed elastic moduli and parameters at various applied pressures with the available published data. At zero pressure, $FrCaCl_3$, $KCaCl_3$, $CsCaCl_3$, $FrGeCl_3$, and $FrSnCl_3$ demonstrate closely aligned values for elastic moduli and parameters. The observed increase in mechanical characteristics, such as Young's modulus (E), bulk modulus (B), and shear modulus (G) values with increasing applied pressure indicate that hardness is incorporated into $FrCaCl_3$ by the applied hydrostatic pressure. Poisson's ratio (ν), as well as Pugh's ratio (B/G), are critical parameters that reveal a material's ductile or brittle characteristics [124,125]. Using the values of B and G, the following elastic parameters can be computed.

$$\text{Pugh's ratio} = \frac{B}{G}$$

$$\text{Poisson's ratio, } v = \frac{3B - 2G}{2(3B + G)}$$

For determining the brittle/ductile nature, the marginal values of ν and B/G are 0.26 and 1.75, correspondingly [50,57,73,74]. A material is regarded as ductile if B/G and ν exceed the marginal value; or else, it is brittle. $FrCaCl_3$ is found ductile material at zero pressure condition, as indicated by the predicted values of ν and B/G (Table 5). The variations in Pugh's ratio and Poisson's ratio of $FrCaCl_3$ under pressure is seen in Fig. 10. It is evident from Fig. 10 that $FrCaCl_3$ becomes more ductile when subjected to pressure. In order to validate the existence of a central force within the crystal, the value of ν must also fall between the ranges of 0.25 and 0.5 [126]. As shown in Table 5, there is a central force within $FrCaCl_3$ since the value of ν falls around 0.25 and 0.5 across the whole pressure range.

Elastic anisotropy (A) offers crucial information on the functionality of materials in various real-world applications [127,128]. It is determined using the Zener equation [129] given below and is displayed in Table 5. A material is considered isotropic if the amount of 'A' equals unity. However, the departure from unity or any value above it indicates the level of anisotropy [130].

$$A = \frac{2C_{44}}{C_{11} - C_{12}}$$

From Tables 5, it is obvious that $FrCaCl_3$ shows anisotropy at zero pressure. Under hydrostatic pressure, it is evidently seen that the value of A rapidly deviates from unity, which suggests that $FrCaCl_3$ is more anisotropic. The direction dependency of Young's modulus (E), shear modulus (G), and Poisson's ratio (ν) at both zero and 150 GPa pressure are shown in both 2D and 3D graphics in Fig. 11. These figures are illustrated using the ELATE tool [91,92,122,123] to visualize the anisotropic character of $FrCaCl_3$. The XY plane is used for projections whereas the XY, YZ, and ZX planes are used to construct the 2D contour plots. The 2D and 3D contour plots of the examined $FrCaCl_3$ make it abundantly evident that it exhibits anisotropy in every possible direction. However, circular 2D and spherical 3D deviations are more severe at 150 GPa pressure than under zero GPa pressure, suggesting that hydrostatic pressure causes higher anisotropy in $FrCaCl_3$.

Direct band gap non-toxic semiconducting halide perovskite materials are highly promising for a range of optoelectronic applications due to several inherent advantages [131,132]. The ability to customize perovskite materials through their versatile and tunable band gap further solidifies their crucial role in advancing optoelectronics [133,134]. This adaptability allows for the tailoring of these materials to meet the needs of specific applications [135,136]. A key benefit lies in their efficient absorption of light, leveraging direct band gaps to enhance the conversion of photons into electron-hole pairs. Fr-based perovskites, distinct from their Pb-based counterparts, offer unique theoretical advantages. Francium, being the heaviest and most electropositive alkali metal, introduces intriguing electronic and structural properties that could potentially lead to novel behaviors in optoelectronics and provide deeper insights into perovskite chemistry. While Pb-based halide perovskites demonstrate high efficiency and favorable optoelectronic characteristics
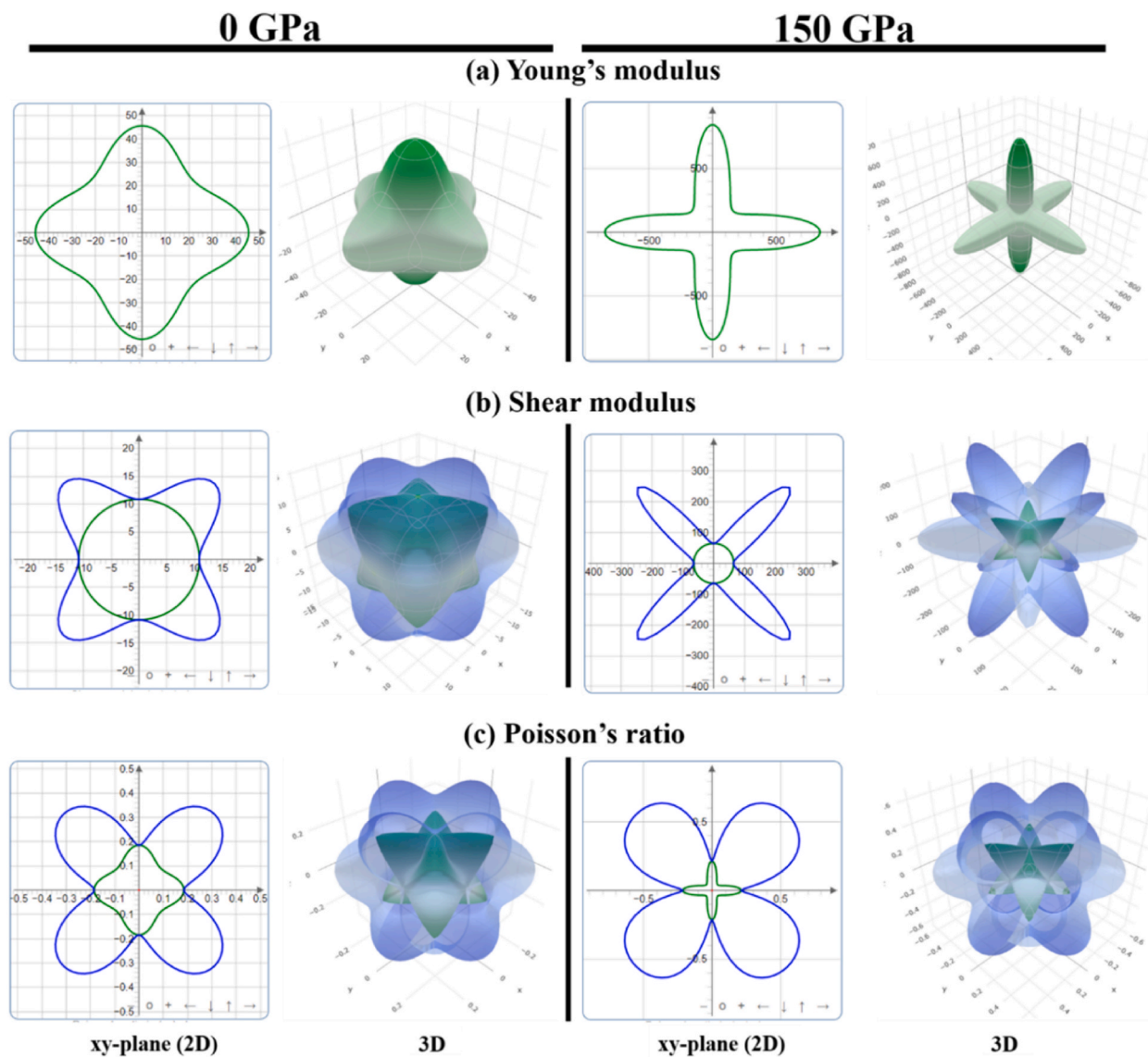
Fig. 11. The anisotropic 3D representation of **(a)** Young's modulus **(b)** Shear modulus, and **(c)** Poisson's ratio of FrCaCl$_3$ at zero GPa, and 150 GPa pressure.

[132], their practical use is hindered by significant drawbacks. Foremost among these is their toxicity, which poses environmental and health risks throughout their lifecycle—from production through to disposal. Moreover, these materials are prone to rapid degradation upon exposure to moisture, oxygen, and heat, limiting their reliability and long-term viability in applications such as solar cells and LEDs.

Despite its radioactivity, Francium halide perovskites have been selected for research due to their unique properties and potential contributions to understanding heavy alkali metals within perovskite frameworks. Additionally, perovskite compositions incorporating radioactive Fr, like FrCaCl$_3$, hold promise for applications in fields such as nuclear medicine, diagnostics, and advanced X-ray imaging technologies [137].

This study emphasizes not only theoretical investigation but also the critical need for experimental confirmation, which forms the bedrock for potential real-world applications. Its impact extends far beyond academia, offering exciting prospects for progress in materials science and technology.

4. Conclusion

The geometry optimization and physical characterization of the FrCaCl$_3$ cubic perovskite are performed using the DFT-based first-principles computational approach. The calculation of the Goldschmidt tolerance factor, octahedral factor, and formation energy

confirms that cubic $FrCaCl_3$ is structurally stable. It is found that induced pressure causes a reduction in the computed lattice constant, unit cell volume, band gap, and chemical bond lengths. Under hydrostatic pressure, the lattice constant of the relaxed structure of cubic $FrCaCl_3$ decreases from 5.487 (5.116) to 4.111 (4.070) Å when employing the GGA-PBE (hybrid HSE06) potential. The utilization of the hybrid HSE06 potential enhances the precision of the band gap, demonstrating a reduction in values from 5.705 to 2.618 eV across pressure ranges of 0–150 GPa. At a pressure of 30 GPa, the indirect band gap transforms into a direct band gap. The band gap narrowing under increased pressure was verified by depicting the density of states (DOS) and the specific projection of electronic contributions from atomic orbitals. This narrowing of the band gap from the UV to the visible area increases the possibility of using $FrCaCl_3$ in optoelectronic devices. According to the structural and optical analyses, this material is predicted to be used in photoconductor-based QLEDs, OLEDs, X-ray detectors, scintillator applications, microelectronics, integrated circuits, waveguides, solar cells, and other optoelectronic devices. Despite being radioactive, Fr is proven to be mechanically stable in nature, and the researched materials may readily be formed into thin films because of their low bulk modulus at zero pressure. The Poisson's ratio (ν) increases from 0.262 to 0.372, and Pugh's ratio (B/G) increases from 1.77 to 3.59, under pressure. Thus, the application of external pressure further induces notable alterations in the mechanical properties, enhancing both ductility and anisotropy in the compound. The intended study would give the research community a thorough scientific grasp and in-depth knowledge of the selected system.

Data availability

Data will be made available on request.

Funding

CRediT authorship contribution statement

Md Istiaque Ahmed: Writing – original draft, Methodology, Investigation, Data curation. **Arpon Biswas:** Formal analysis, Data curation. **Tariqul Islam Asif:** Formal analysis, Data curation. **Md Saiduzzaman:** Writing – review & editing, Writing – original draft, Supervision, Formal analysis, Conceptualization. **Minhajul Islam:** Writing – review & editing, Writing – original draft, Validation, Formal analysis, Data curation.

Declaration of competing interest

The authors declare that they have no known competing financial interests or personal relationships that could have appeared to influence the work reported in this paper.

Acknowledgements

References

[1] M.A. Islam, Jakiul Islam, M. Nazrul Islam, Sapan Kumar Sen, A.K.M. Hossain, Enhanced ductility and optoelectronic properties of environment-friendly $CsGeCl_3$ under pressure, AIP Adv. 11 (4) (2021) 045014, https://doi.org/10.1063/5.0048849.

[2] Y. Huang, L. Wang, Z. Ma, F. Wang, Pressure-induced band structure evolution of halide perovskites: a first-principles atomic and electronic structure study, J. Phys. Chem. C 123 (2019) 739–745, https://doi.org/10.1021/acs.jpcc.8b11500.

[3] R.Y. Alyoubi, B.M. Raffah, F. Hamioud, A.A. Mubarak, Effect of pressure on the mechanical, electronic and optical characters of $CsSnBr_3$ and $CsSnI_3$: ab-initio study, Mod. Phys. Lett. B 35 (2021) 2150056, https://doi.org/10.1142/s0217984921500561.

[4] S. Yalameha, P. Saeidi, Z. Nourbakhsh, A. Vaez, A. Ramazani, Insight into the topological phase and elastic properties of halide perovskites $CsSnX_3$ (X = I, Br, Cl) under hydrostatic pressures, J. Appl. Phys. 127 (2020) 085102, https://doi.org/10.1063/1.5125920.

[5] A. Bernasconi, A. Rizzo, A. Listorti, A. Mahata, E. Mosconi, F. de Angelis, L. Malavasi, Synthesis, properties, and modeling of $Cs_{1-x}Rb_xSnBr_3$ solid solution: a new mixed-cation lead-free all-inorganic perovskite system, Chem. Mater. 31 (2019) 3527–3533, https://doi.org/10.1021/acs.chemmater.9b00837.

[6] T.C. Jellicoe, J.M. Richter, H.F.J. Glass, M. Tabachnyk, R. Brady, S.E. Dutton, A. Rao, R.H. Friend, D. Credgington, N.C. Greenham, M.L. Böhm, Synthesis and optical properties of lead-free cesium tin halide perovskite nanocrystals, J. Am. Chem. Soc. 138 (2016) 2941–2944, https://doi.org/10.1021/jacs.5b13470.

[7] X.G. Zhao, G.M. Dalpian, Z. Wang, A. Zunger, Polymorphous nature of cubic halide perovskites, Phys. Rev. B 101 (2020) 155137, https://doi.org/10.1103/physrevb.101.155137.

[8] A. Oleaga, A. Salazar, D. Skrzypek, Critical behaviour of magnetic transitions in KCoF3 and KNiF3 perovskites, J. Alloys Compd. 629 (2015) 178–183, https://doi.org/10.1016/J.JALLCOM.2014.12.237.

[9] M. Llanos, R. Yekani, G.P. Demopoulos, N. Basu, Alternatives assessment of perovskite solar cell materials and their methods of fabrication, Renew. Sustain. Energy Rev. 133 (2020) 110207, https://doi.org/10.1016/j.rser.2020.110207.

[10] R. Nie, R.R. Sumukam, S.H. Reddy, M. Banavoth, S. il Seok, Lead-free perovskite solar cells enabled by hetero-valent substitutes, Energy Environ. Sci. 13 (2020) 2363–2385, https://doi.org/10.1039/d0ee01153c.

[11] B. Wu, W. Ning, Q. Xu, M. Manjappa, M. Feng, S. Ye, J. Fu, S. Lie, T. Yin, F. Wang, T.W. Goh, P.C. Harikesh, Y.K.E. Tay, Z.X. Shen, F. Huang, R. Singh, G. Zhou, F. Gao, T.C. Sum, Strong self-trapping by deformation potential limits photovoltaic performance in bismuth double perovskite, Sci. Adv. 7 (2021) eabd3160, https://doi.org/10.1126/sciadv.abd3160.

[12] Z. Lan, J. Meng, K. Zheng, I.E. Castelli, Exploring the intrinsic point defects in cesium copper halides, J. Phys. Chem. C 125 (2021) 1592–1598, https://doi.org/10.1021/acs.jpcc.0c11216.

[13] S.J. Clark, C.D. Flint, J.D. Donaldson, Luminescence and electrical conductivity of CsSnBr$_3$, and related phases, J. Phys. Chem. Solid. 42 (1981) 133–135, https://doi.org/10.1016/0022-3697(81)90072-x.

[14] D. Moghe, L. Wang, C.J. Traverse, A. Redoute, M. Sponseller, P.R. Brown, V. Bulović, R.R. Lunt, All vapor-deposited lead-free doped CsSnBr$_3$ planar solar cells, Nano Energy 28 (2016) 469–474, https://doi.org/10.1016/j.nanoen.2016.09.009.

[15] L.Y. Huang, W.R.L. Lambrecht, Electronic band structure, phonons, and exciton binding energies of halide perovskites CsSnCl$_3$, CsSnBr$_3$, and CsSnI$_3$, Phys. Rev. B 88 (2013) 165203, https://doi.org/10.1103/physrevb.88.165203.

[16] M. Houari, B. Bouadjemi, S. Haid, M. Matougui, T. Lantri, Z. Aziz, S. Bentata, B. Bouhafs, Semiconductor behavior of halide perovskites AGeX$_3$ (A = K, Rb and Cs, Indian J. Phys. 94 (2020) 455–467, https://doi.org/10.1007/s12648-019-01480-0.

[17] M. Saiduzzaman, S. Yanagida, T. Takei, N. Kumada, K. Ogawa, C. Moriyoshi, Y. Kuroiwa, S. Kawaguchi, Crystal structure, thermal behavior, and photocatalytic activity of NaBiO$_3$·nH$_2$O, Inorg. Chem. 57 (2018) 8903–8908, https://doi.org/10.1021/acs.inorgchem.8b00799.

[18] M. Saiduzzaman, T. Takei, S. Yanagida, N. Kumada, H. Das, H. Kyokane, S. Wakazaki, M. Azuma, C. Moriyoshi, Y. Kuroiwa, Hydrothermal synthesis of pyrochlore-type pentavalent bismuthates Ca$_2$Bi$_2$O$_7$ and Sr$_2$Bi$_2$O$_7$, Inorg. Chem. 58 (2019) 1759–1763, https://doi.org/10.1021/acs.inorgchem.8b03596.

[19] M. Saiduzzaman, S. Akutsu, N. Kumada, T. Takei, S. Yanagida, H. Yamane, Y. Kusano, Hydrothermal synthesis and crystal structure of a mixed-valence bismuthate, Na$_3$Bi$_3$O$_8$, Inorg. Chem. 59 (2020) 4950–4960, https://doi.org/10.1021/acs.inorgchem.0c00213.

[20] K.M. Hossain, M. Saiduzzaman, N. Kumada, T. Takei, H. Yamane, M.H. Kabir Rubel, Hydrothermal synthesis and crystal structure of a novel bismuth oxide: (K$_{0.2}$Sr$_{0.8}$)(Na$_{0.01}$Ca$_{0.25}$Bi$_{0.74}$)O$_3$, ACS Omega 6 (2021) 15975–15980, https://doi.org/10.1021/acsomega.1c01694.

[21] M. Saiduzzaman, T. Takei, N. Kumada, Hydrothermal magic for the synthesis of new bismuth oxides, Inorg. Chem. Front. 8 (2021) 2918–2938, https://doi.org/10.1039/D1QI00337B.

[22] M. Islam, DFT and DFT+U insights into the physical properties of UO$_2$, J. Sci. Res. 15 (3) (2023) 739–757, https://doi.org/10.3329/jsr.v15i3.64394.

[23] M.I. Sayyed, B. Albarzan, A.H. Almuqrin, A.M. El-Khatib, A. Kumar, D.I. Tishkevich, A.v. Trukhanov, M. Elsafi, Experimental and theoretical study of radiation shielding features of CaO–K$_2$O–Na$_2$O–P$_2$O$_5$ glass systems, Materials 14 (2021) 3772, https://doi.org/10.3390/ma14143772.

[24] A. Fedotov, V. Shendyukov, L. Tsybulskaya, S. Perevoznikov, M. Dong, X. Xue, X. Feng, M.I. Sayyed, T. Zubar, A. Trukhanov, D. Tishkevich, Electrodeposition conditions-dependent crystal structure, morphology and electronic properties of Bi films, J. Alloys Compd. 887 (2021) 161451, https://doi.org/10.1016/j.jallcom.2021.161451.

[25] M.I. Abbas, J.S. Alzahrani, M.I. Sayyed, D.I. Tishkevich, M.T. Alabsy, A.M. El-Khatib, M. Elsafi, Gamma-ray attenuation and exposure buildup factor of novel polymers in shielding using geant4 simulation, Materials 14 (2021) 5051, https://doi.org/10.3390/ma14175051.

[26] M.H.K. Rubel, S.K. Mitro, B.K. Mondal, M.M. Rahaman, M. Saiduzzaman, J. Hossain, A.K.M.A. Islam, N. Kumada, Newly synthesized A-site ordered cubic-perovskite superconductor (Ba$_{0.54}$K$_{0.46}$)$_4$Bi$_4$O$_{12}$: a DFT investigation, Physica C 574 (2020) 1353669, https://doi.org/10.1016/j.physc.2020.1353669.

[27] M.A. Haq, M. Saiduzzaman, T.I. Asif, I.K. Shuvo, K.M. Hossain, Ultra-violet to visible band gap engineering of cubic halide KCaCl$_3$ perovskite under pressure for optoelectronic applications: insights from DFT, RSC Adv. 11 (2021) 36367–36378, https://doi.org/10.1039/d1ra06430d.

[28] Shafiqul Islam Faisal, Abi Muttaquin Bin Jalal Bayar, Gamma shielding experiment simulation utilizing MCNPX code, J. Eng. Sci. 12 (2021) 11–21, https://doi.org/10.3329/jes.v12i2.54627.

[29] Y.G. Shi, Y.F. Guo, S. Yu, M. Arai, A.A. Belik, A. Sato, K. Yamaura, E. Takayama-Muromachi, H.F. Tian, H.X. Yang, J.Q. Li, T. Varga, J.F. Mitchell, S. Okamoto, Continuous metal-insulator transition of the antiferromagnetic perovskite NaOsO$_3$, Phys. Rev. B 80 (R) (2009) 161104, https://doi.org/10.1103/physrevb.80.161104.

[30] C.C. Stoumpos, C.D. Malliakas, J.A. Peters, Z. Liu, M. Sebastian, J. Im, T.C. Chasapis, A.C. Wibowo, D.Y. Chung, A.J. Freeman, B.W. Wessels, M.G. Kanatzidis, Crystal growth of the perovskite semiconductor CsPbBr$_3$: a new material for high-energy radiation detection, Cryst. Growth Des. 13 (2013) 2722–2727, https://doi.org/10.1021/cg400645t.

[31] A.N. Baranov, D.C. Kim, J.S. Kim, H.R. Kang, Y.W. Park, J.S. Pshirkov, E.v. Antipov, Superconductivity in the Ba$_{1-x}$K$_x$BiO$_3$ system, Phys. C Supercond. Appl. (2001) 414–417, https://doi.org/10.1016/s0921-4534(01)00263-5.

[32] P. Goel, S. Sundriyal, V. Shrivastav, S. Mishra, D.P. Dubal, K.H. Kim, A. Deep, Perovskite materials as superior and powerful platforms for energy conversion and storage applications, Nano Energy 80 (2021) 105552, https://doi.org/10.1016/j.nanoen.2020.105552.

[33] A.S. Bhalla, R. Guo, R. Roy, The perovskite structure—a review of its role in ceramic science and technology, Mater. Res. Innov. 4 (2000) 3–26, https://doi.org/10.1007/s100190000062.

[34] J. Sunarso, S.S. Hashim, N. Zhu, W. Zhou, Perovskite oxides applications in high temperature oxygen separation, solid oxide fuel cell and membrane reactor: a review, Prog. Energy Combust. Sci. 61 (2017) 57–77, https://doi.org/10.1016/j.pecs.2017.03.003.

[35] P. Kanhere, Z. Chen, A review on visible light active perovskite-based photocatalysts, Molecules 19 (2014) 19995–20022, https://doi.org/10.3390/molecules191219995.

[36] J. Tian, Q. Xue, Q. Yao, N. Li, C.J. Brabec, H.L. Yip, Inorganic halide perovskite solar cells: progress and challenges, Adv. Energy Mater. 10 (2020) 2000183, https://doi.org/10.1002/aenm.202000183.

[37] C. Gómez-Solís, J. Oliva, L.A. Diaz-Torres, J. Bernal-Alvarado, V. Reyes-Zamudio, A. Abidov, L.M. Torres-Martinez, Efficient photocatalytic activity of MSnO$_3$ (M: Ca, Ba, Sr) stannates for photoreduction of 4-nitrophenol and hydrogen production under UV light irradiation, J. Photochem. Photobiol., A 371 (2019) 365–373, https://doi.org/10.1016/j.jphotochem.2018.11.039.

[38] W. Dong, B. Li, Y. Li, X. Wang, L. An, C. Li, B. Chen, G. Wang, Z. Shi, General approach to well-defined perovskite MTiO$_3$ (M = Ba, Sr, Ca, and Mg) nanostructures, J. Phys. Chem. C 115 (2011) 3918–3925, https://doi.org/10.1021/jp110660v.

[39] J. Jia, S. Guo, S. Yan, F. Cao, C. Yao, X. Dong, G. Wang, Simultaneous large pyroelectric response and high depolarization temperature in sodium bismuth titanate-based perovskites, Appl. Phys. Lett. 114 (2019) 032902, https://doi.org/10.1063/1.5063318.

[40] K. Wieczorek, A. Ziebiniska, Z. Ujma, K. Szot, M. Górny, I. Franke, J. Koperski, A. Soszyński, K. Roleder, Electrostrictive and piezoelectric effect in BaTiO$_3$ and PbZrO$_3$, Ferroelectrics 336 (2006) 61–67, https://doi.org/10.1080/00150190600695743.

[41] R.M. Kusters, J. Singleton, D.A. Keen, R. McGreevy, W. Hayes, Magnetoresistance measurements on the magnetic semiconductor Nd$_{0.5}$Pb$_{0.5}$MnO$_3$, Phys. B Condens. Matter 155 (1989) 362–365, https://doi.org/10.1016/0921-4526(89)90530-9.

[42] H. Hayashi, H. Inaba, M. Matsuyama, N.G. Lan, M. Dokiya, H. Tagawa, Structural consideration on the ionic conductivity of perovskite-type oxides, Solid State Ionics 122 (1999) 1–15, https://doi.org/10.1016/s0167-2738(99)00066-1.

[43] M. Yaseen, M.K. Butt, A. Ashfaq, J. Iqbal, M.M. Almoneef, Misbah, M. Iqbal, A. Murtaza, A. Laref, Phase transition and thermoelectric properties of cubic KNbO$_3$ under pressure: DFT approach, J. Mater. Res. Technol. 11 (2021) 2106–2113, https://doi.org/10.1016/j.jmrt.2021.02.017.

[44] N.A. Noor, M. Rashid, G.M. Mustafa, M.I. Khan, A. Mahmood, S.M. Ramay, Study of pressure induced physical properties of ZnZrO$_3$ perovskite using density functional theory, Chem. Phys. Lett. 753 (2020) 137601, https://doi.org/10.1016/j.cplett.2020.137601.

[45] N.A. Noor, M. Rashid, S.M. Alay-E-Abbas, M. Raza, A. Mahmood, S.M. Ramay, G. Murtaza, Shift of indirect to direct bandgap and thermoelectric response of the cubic BiScO$_3$ via DFT-mBJ studies, Mater. Sci. Semicond. Process. 49 (2016) 40–47, https://doi.org/10.1016/j.mssp.2016.03.014.

[46] S.S.A. Gillani, R. Ahmad, I. Zeba, Islah u-din, M. Rizwan, M. Rafique, M. Shakil, S. Jabbar, M. Siddique, Structural stability of SrZrO$_3$ perovskite and improvement in electronic and optical properties by Ca and Ba doping for optoelectronic applications: a DFT approach, Phil. Mag. Lett. 99 (2019) 3133–3145, https://doi.org/10.1080/14786435.2019.1663955.

[47] N.H. Linh, N.H. Tuan, D.D. Dung, P.Q. Bao, B.T. Cong, L.T.H. Thanh, Alkali metal-substituted bismuth-based perovskite compounds: a DFT study, J. Sci. Adv. Mater. Devices 4 (2019) 492–498, https://doi.org/10.1016/j.jsamd.2019.06.005.

[48] M. Yaseen, H. Shafiq, J. Iqbal, Misbah, F. Batool, A. Murtaza, M. Iqbal, H. Althib, S.M. Ramay, A. Mahmood, Pressure induced electronic, optical and thermoelectric properties of cubic SrZrO$_3$: DFT investigation, Phys. B Condens. Matter 612 (2021) 412626, https://doi.org/10.1016/j.physb.2020.412626.

[49] J. Islam, A.K.M.A. Hossain, Semiconducting to metallic transition with outstanding optoelectronic properties of CsSnCl$_3$ perovskite under pressure, Sci. Rep. 10 (2020) 14391, https://doi.org/10.1038/s41598-020-71223-3.

[50] M.A. Islam, J. Islam, M.N. Islam, S.K. Sen, A.K.M.A. Hossain, Enhanced ductility and optoelectronic properties of environment-friendly CsGeCl$_3$ under pressure, AIP Adv. 11 (2021), https://doi.org/10.1063/5.0048849.

[51] M.S. Hossain, M.M. Haque Babu, T. Saha, M.S. Hossain, J. Podder, M.S. Rana, A. Barik, P. Rani, Pressure induced semiconductor to metal phase transition in cubic CsSnBr$_3$ perovskite, AIP Adv. 11 (2021) 055024, https://doi.org/10.1063/5.0048979.

[52] G. Murtaza, I. Ahmad, A. Afaq, Shift of indirect to direct bandgap in going from K to Cs in MCaF$_3$ (M = K, Rb, Cs), Solid State Sci. 16 (2013) 152–157, https://doi.org/10.1016/j.solidstatesciences.2012.10.002.

[53] S.S.A. Gillani, R. Ahmad, M. Rizwan, M. Rafique, G. Ullah, C.B. Cao, H.B. Jin, Effect of magnesium doping on band gap and optical properties of SrZrO$_3$ perovskite: a first-principles study, Optik 191 (2019) 132–138, https://doi.org/10.1016/j.ijleo.2019.05.099.

[54] K.M. Hossain, M. Zahid Hasan, M. Lokman Ali, Understanding the influences of Mg doping on the physical properties of SrMoO$_3$ perovskite, Results Phys. 19 (2020) 103337, https://doi.org/10.1016/j.rinp.2020.103337.

[55] M.N. Islam, M.A. Hadi, J. Podder, Influence of Ni doping in a lead-halide and a lead-free halide perovskites for optoelectronic applications, AIP Adv. 9 (2019), https://doi.org/10.1063/1.5132985.

[56] M.Z. Rahaman, A.K.M.A. Hossain, Effect of metal doping on the visible light absorption, electronic structure and mechanical properties of non-toxic metal halide CsGeCl$_3$, RSC Adv. 8 (58) (2018) 33010–33018, https://doi.org/10.1039/C8RA06374E.

[57] M.A.H. Shah, et al., Hydrostatic pressure on XLiH$_3$ (X= Ba, Sr, Ca) perovskite hydrides: an insight into structural, thermo-elastic and ultrasonic properties through first-principles investigation, Solid State Commun. 328 (2021) 114222, https://doi.org/10.1016/j.ssc.2021.114222.

[58] M.I. Kholil, M.T.H. Bhuiyan, M.A. Rahman, M.S. Ali, M. Aftabuzzaman, Influence of molybdenum and technetium doping on visible light absorption, optical and electronic properties of lead-free perovskite CsSnBr$_3$ for optoelectronic applications, RSC Adv. 11 (2021) 2405–2414, https://doi.org/10.1039/d0ra09853a.

[59] H. Chen, C. Tan, D. Sun, W. Zhao, X. Tian, Y. Huang, Ultrawide range tuning of direct band gap in MgZnO monolayer via electric field effect, RSC Adv. 8 (2018) 1392–1397, https://doi.org/10.1039/c7ra11766c.

[60] Y. Li, J. Chen, C. Zhao, Influence of external electric field on the electronic structure and optical properties of pyrite, RSC Adv. 7 (2017) 56676–56681, https://doi.org/10.1039/c7ra10815j.

[61] H. Kobayashi, Pressure-induced semiconductor-metal-semiconductor transitions in FeS, Phys. Rev. B 63 (2001) 115203, https://doi.org/10.1103/PhysRevB.63.115203.

[62] A.P. Nayak, S. Bhattacharyya, J. Zhu, J. Liu, X. Wu, T. Pandey, C. Jin, A.K. Singh, D. Akinwande, J.F. Lin, Pressure-induced semiconducting to metallic transition in multilayered molybdenum disulphide, Nat. Commun. 5 (2014) 3731, https://doi.org/10.1038/ncomms4731.

[63] I. Ahmed, F. Parvin, A.K.M.A. Islam, M.A. Kashem, Inverse-perovskites Sc$_3$GaX (X= B, C, N): a comprehensive theoretical investigation at ambient and elevated pressures, Computational Condensed Matter 35 (2023) e00808, https://doi.org/10.1016/j.cocom.2023.e00808.

[64] N.A. Noor, Q. Mahmood, M. Rashid, B. Ul Haq, A. Laref, The pressure-induced mechanical and optoelectronic behavior of cubic perovskite PbSnO$_3$ via ab-initio investigations, Ceram. Int. 44 (2018) 13750–13756, https://doi.org/10.1016/j.ceramint.2018.04.217.

[65] M.A. Alam, M.A.H. Shah, M. Nuruzzaman, M.A. Hadi, F. Parvin, M.A.K. Zilani, Effect of hydrostatic compression on physical properties of Li$_2$TmSi$_3$ (Tm= Ir, Pt, Rh, Os) with ground-state optical features, J. Phys. Chem. Solid. 156 (2021) 110124, https://doi.org/10.1016/j.jpcs.2021.110124.

[66] A. Batool, M.A. Faridi, Q. Mahmood, B. Ul Haq, A. Laref, S.E. Awan, The pressure-induced indirect to direct bandgap transition and thermoelectric response in SrTiO$_3$: an ab-initio study, J. Phys. Chem. Solid. 123 (2018) 70–75, https://doi.org/10.1016/j.jpcs.2018.07.008.

[67] B. Liu, Y. Han, C. Gao, Y. Ma, G. Peng, B. Wu, C. Liu, Y. Wang, T. Hu, X. Cui, W. Ren, Y. Li, N. Su, H. Liu, G. Zou, Pressure induced semiconductor-semimetal transition in WSe$_2$, J. Phys. Chem. C 114 (2010) 14251–14254, https://doi.org/10.1021/jp104143e.

[68] S. Tongay, J. Zhou, C. Ataca, K. Lo, T.S. Matthews, J. Li, J.C. Grossman, J. Wu, Thermally driven crossover from indirect toward direct bandgap in 2D semiconductors: MoSe$_2$ versus MoS$_2$, Nano Lett. 12 (2012) 5576–5580, https://doi.org/10.1021/nl302584w.

[69] M. Abdul Hadi Shah, A. Hossain, M. Ashraful Alam, M. Sarwar Pervez, M. Nuruzzaman, M.A.K. Zilani, Exploring pressure induced thermoelectric properties of LiAeH$_3$ (Ae= Ca, Sr, Ba) perovskite hydrides along with optoelectronic features, Mater. Sci. Semicond. Process. 137 (2022) 106238, https://doi.org/10.1016/j.mssp.2021.106238.

[70] M.N. Islam, J. Podder, T. Saha, P. Rani, Semiconductor to metallic transition under induced pressure in Cs$_2$AgBiBr$_6$ double halide perovskite: a theoretical DFT study for photovoltaic and optoelectronic applications, RSC Adv. 11 (2021) 24001–24012, https://doi.org/10.1039/D1RA03161A.

[71] M.A.H. Shah, M. Nuruzzaman, A. Hossain, M. Jubair, M.A.K. Zilani, A DFT insight into structural, mechanical, elasto-acoustic, and anisotropic properties of AePdH$_3$ (Ae= Ca, Sr, Ba) perovskites under pressure, Computational Condensed Matter 34 (2023) e00774, https://doi.org/10.1016/j.cocom.2022.e00774.

[72] M. Hassan, I. Arshad, Q. Mahmood, Computational study of electronic, optical and thermoelectric properties of X$_3$PbO (X= Ca, Sr, Ba) anti-perovskites, Semicond. Sci. Technol. 32 (2017) 115002, https://doi.org/10.1088/1361-6641/aa8afe.

[73] M.S. Hossain, M.M. Haque Babu, T. Saha, M.S. Hossain, J. Podder, M.S. Rana, A. Barik, P. Rani, Pressure induced semiconductor to metal phase transition in cubic CsSnBr$_3$ perovskite, AIP Adv. 11 (2021), https://doi.org/10.1063/5.0048979.

[74] M.A. Islam, M.Z. Rahaman, S.K. Sen, A comparative study of hydrostatic pressure treated environmentally friendly perovskites CsXBr$_3$ (X = Ge/Sn) for optoelectronic applications, AIP Adv. 11 (2021), https://doi.org/10.1063/5.0057287.

[75] A.A. Mubarak, The elastic, electronic and optical properties of RbCaX$_3$ (X= F, Cl) compounds, Int. J. Mod. Phys. B 28 (2014) 1450192, https://doi.org/10.1142/S0217979214501926.

[76] A.A. Mousa, First-principles study of structural, electronic and optical properties of the KCaX$_3$ (X = F and Cl) compounds, Int. J. Mod. Phys. B 28 (2014), https://doi.org/10.1142/S0217979214501392.

[77] K. Ephraim Babu, N. Murali, K. Vijaya Babu, P.T. Shibeshi, V. Veeraiah, Structural, elastic, electronic, and optical properties of cubic perovskite CsCaCl$_3$ compound: an ab initio study, Acta Phys. Pol., A 125 (2014) 1179–1185, https://doi.org/10.12693/APhysPolA.125.1179.

[78] D. Ray, C. Clark, H.Q. Pham, J. Borycz, R.J. Holmes, E.S. Aydil, L. Gagliardi, Computational study of structural and electronic properties of lead-free CsMI$_3$ perovskites (M = Ge, Sn, Pb, Mg, Ca, Sr, and Ba), J. Phys. Chem. C 122 (2018) 7838–7848, https://doi.org/10.1021/ACS.JPCC.8B00226.

[79] T. Nishimatsu, N. Terakubo, H. Mizuseki, Y. Kawazoe, D.A. Pawlak, K. Shimamura, T. Fukuda, Band structures of perovskite-like fluorides for vacuum-ultraviolet-transparent lens materials, Jpn. J. Appl. Phys. 41 (2002), https://doi.org/10.1143/JJAP.41.L365/META. Part 2: Letters.

[80] I. Zeba, R. Kiran, M. Shakil, M. Rafique, Riaz Ahmad, S.S.A. Gillani, Study the effect of magnesium doping concentration on structural and optoelectronic response of NaCa$_{1-x}$Mg$_x$F$_3$ fluoro-perovskite: first-principles computation, Optik 218 (2020) 164990, https://doi.org/10.1016/j.ijleo.2020.164990.

[81] L. Li, Y.J. Wang, D.X. Liu, C.G. Ma, M.G. Brik, A. Suchocki, M. Piasecki, A.H. Reshak, Comparative first-principles calculations of the electronic, optical, elastic and thermodynamic properties of XCaF$_3$ (X = K, Rb, Cs) cubic perovskites, Mater. Chem. Phys. 188 (2017) 39–48, https://doi.org/10.1016/J.MATCHEMPHYS.2016.12.033.

[82] S. Soleimanpour, F. Kanjouri, Elastic, electronic and optical properties of the cubic fluoro-perovskite KCaF$_3$ under pressure, Indian J. Phys. 89 (2015) 687–697, https://doi.org/10.1007/S12648-014-0635-Y.

[83] B. Ghebouli, M.A. Ghebouli, A. Bouhemadou, M. Fatmi, R. Khenata, D. Rached, T. Ouahrani, S. Bin-Omran, Theoretical prediction of the structural, elastic, electronic, optical and thermal properties of the cubic perovskites CsXF$_3$ (X = Ca, Sr and Hg) under pressure effect, Solid State Sci. 14 (2012) 903–913, https://doi.org/10.1016/J.SOLIDSTATESCIENCES.2012.04.019.

[84] N. Hasan, M. Arifuzzaman, A. Kabir, Structural, elastic and optoelectronic properties of inorganic cubic FrBX$_3$ (B = Ge, Sn; X = Cl, Br, I) perovskite: the density functional theory approach, RSC Adv. 12 (2022) 7961–7972, https://doi.org/10.1039/D2RA00546H.

[85] M.D. Segall, P.J.D. Lindan, M.J. Probert, C.J. Pickard, P.J. Hasnip, S.J. Clark, M.C. Payne, First-principles simulation: ideas, illustrations and the CASTEP code, J. Condens. Mat. Phys. 14 (2002) 2717, https://doi.org/10.1088/0953-8984/14/11/301.

[86] John P. Perdew, Kieron Burke, Matthias Ernzerhof, Generalized gradient approximation made simple, Phys. Rev. Lett. 77 (18) (1996) 3865, https://doi.org/10.1103/PhysRevLett.77.3865.

[87] D. Vanderbilt, Soft self-consistent pseudopotentials in a generalized eigenvalue formalism, Phys. Rev. B 41 (1990) 7892, https://doi.org/10.1103/PhysRevB.41.7892.

[88] H.J. Monkhorst, J.D. Pack, Special points for Brillouin-zone integrations, Phys. Rev. B 13 (1976) 5188, https://doi.org/10.1103/physrevb.13.5188.

[89] T.H. Fischer, J. Almlöf, General methods for geometry and wave function optimization, J. Phys. Chem. 96 (1992) 9768–9774, https://doi.org/10.1021/J100203A036.

[90] K. Momma, F. Izumi, VESTA 3 for three-dimensional visualization of crystal, volumetric and morphology data, J. Appl. Crystal. 44 (2011) 1272–1276, https://doi.org/10.1107/s0021889811038970.

[91] R. Gaillac, P. Pullumbi, F, C, ELATE: an Open-Source Online Application for Analysis and Visualization of Elastic Tensors, Iopscience, 2016, https://doi.org/10.1088/0953-8984/28/27/275201. J. of Physics, undefined 2016.

[92] Minhajul Islam, A comparative investigation on the fundamental physical properties of UX_2 (X = O, N, C, Si and S) solid nuclear fuel materials: a DFT+U study, Chemical Physics Impact 7 (2023) 100310, https://doi.org/10.1016/j.chphi.2023.100310.

[93] S. Bhattacharyya, A.K. Singh, Semiconductor-metal transition in semiconducting bilayer sheets of transition-metal dichalcogenides, Phys. Rev. B 86 (2012), https://doi.org/10.1103/physrevb.86.075454, 075454–075454.

[94] J. Islam, A.K.M.A. Hossain, Semiconducting to metallic transition with outstanding optoelectronic properties of $CsSnCl_3$ perovskite under pressure, Sci. Rep. 10 (2020), https://doi.org/10.1038/S41598-020-71223-3.

[95] A.A. Mousa, M.S. Abu-Jafar, D. Dahliah, R.M. Shaltaf, J.M. Khalifeh, Investigation of the perovskite $KSrX_3$ (X = Cl and F) compounds, examining the optical, elastic, electronic and structural properties: FP-LAPW study, J. Electron. Mater. 47 (2017) 641–650, https://doi.org/10.1007/S11664-017-5817-X.

[96] G. Shwetha, V. Kanchana, Optical isotropy in structurally anisotropic halide scintillators: *Ab initio* study, Phys. Rev. B Condens. Matter 86 (2012) 115209, https://doi.org/10.1103/PhysRevB.86.115209.

[97] Jahid Kabir Rony, Minhajul Islam, Md Saiduzzaman, Khandaker Monower Hossain, Safin Alam, Arpon Biswas, M.H. Mia, Sohail Ahmad, S.K. Mitro, $TlBX_3$ (B = Ge, Sn; X = Cl, Br, I): promising non-toxic metal halide perovskites for scalable and affordable optoelectronics, J. Mater. Res. Technol. 29 (2024) 897–909, https://doi.org/10.1016/j.jmrt.2024.01.093.

[98] Shariare Hossain Rabbi, Tariqul Islam Asif, Md Istiaque Ahmed, Md Saiduzzaman, Minhajul Islam, Unveiling the pressure-driven modulations in $AGeF_3$ (A= Na, Tl) cubic perovskite halides for enhanced optoelectronic performance, Computational Condensed Matter 38 (2024) e00887, https://doi.org/10.1016/j.cocom.2024.e00887.

[99] J. Islam, A.K.M.A. Hossain, Semiconducting to metallic transition with outstanding optoelectronic properties of $CsSnCl_3$ perovskite under pressure, Sci. Rep. 10 (2020) 1–11, https://doi.org/10.1038/S41598-020-71223-3.

[100] M.I. Kholil, M.T.H. Bhuiyan, Effects of pressure on narrowing the band gap, visible light absorption, and semi-metallic transition of lead-free perovskite $CsSnBr_3$ for optoelectronic applications, J. Phys. Chem. Solid. 154 (2021), https://doi.org/10.1016/J.JPCS.2021.110083.

[101] M. Yaseen, H. Shafiq, J. Iqbal, Misbah, F. Batool, A. Murtaza, M. Iqbal, H. Althib, S.M. Ramay, A. Mahmood, Pressure induced electronic, optical and thermoelectric properties of cubic $SrZrO_3$: DFT investigation, Physica B: Condens. Matter 612 (2021), https://doi.org/10.1016/J.PHYSB.2020.412626.

[102] S.S.A. Gillani, R. Ahmad, I. Zeba, Islah u-din, M. Shakil, M. Rizwan, M. Rafique, M. Sarfraz, S.S. Hassan, Effect of external pressure on the structural stability, electronic structure, band gap engineering and optical properties of $LiNbO_3$: an *ab-initio* calculation, Mater. Today Commun. 23 (2020), https://doi.org/10.1016/J.MTCOMM.2020.100919.

[103] G. Shwetha, V. Kanchana, Optical isotropy in structurally anisotropic halide scintillators: *Ab initio* study, Phys. Rev. B 86 (2012) 115209, https://doi.org/10.1103/PhysRevB.86.115209.

[104] K.M. Hossain, M.Z. Hasan, M.L. Ali, Narrowing bandgap and enhanced mechanical and optoelectronic properties of perovskite halides: effects of metal doping, AIP Adv. 11 (2021) 015052, https://doi.org/10.1063/5.0039308.

[105] N. Hasan, M. Arifuzzaman, A. Kabir, Structural, elastic and optoelectronic properties of inorganic cubic $FrBX_3$ (B= Ge, Sn; X= Cl, Br, I) perovskite: the density functional theory approach, RSC Adv. 12 (2022) 7961–7972, https://doi.org/10.1039/d2ra00546h.

[106] G. Yu, C.H. Lee, A.J. Heeger, S.W. Cheong, Photoconductivity and optical conductivity in lightly doped $Nd_2CuO_{4-\delta}$, Physica C Supercond 203 (1992) 419–425, https://doi.org/10.1016/0921-4534(92)90051-D.

[107] M. Roknuzzaman, K.K. Ostrikov, H. Wang, A. Du, T. Tesfamichael, Towards lead-free perovskite photovoltaics and optoelectronics by ab-initio simulations, Sci. Rep. 7 (2017) 1–8, https://doi.org/10.1038/s41598-017-13172-y.

[108] M.M. Rahaman, M.H.K. Rubel, M.A. Rashid, M.A. Alam, K.M. Hossain, M.I. Hossain, A.A. Khatun, M.M. Hossain, A.K.M.A. Islam, S. Kojima, N. Kumada, Mechanical, electronic, optical, and thermodynamic properties of orthorhonmbic $LiCuBiO4$ crystal: a first-priciples study, J. Mater. Res. Technol. 8 (2019) 3783–3794, https://doi.org/10.1016/J.JMRT.2019.06.039.

[109] M. Roknuzzaman, K. (Ken) Ostrikov, K. Chandula Wasalathilake, C. Yan, H. Wang, T. Tesfamichael, Insight into lead-free organic-inorganic hybrid perovskites for photovoltaics and optoelectronics: a first-principles study, Org. Electron. 59 (2018) 99–106, https://doi.org/10.1016/J.ORGEL.2018.04.051.

[110] M.I. Naher, S.H. Naqib, Structural, elastic, electronic, bonding, and optical properties of topological $CaSn_3$ semimetal, J. Alloys Compd. 829 (2020) 154509, https://doi.org/10.1016/j.jallcom.2020.154509.

[111] X. Liu, B. Xie, C. Duan, Z. Wang, B. Fan, K. Zhang, B. Lin, F.J. Colberts, W. Ma, R.A. Janssen, A high dielectric constant non-fullerene acceptor for efficient bulk-heterojunction organic solar cells, J. Mater. Chem. A 6 (2018) 395–403, https://doi.org/10.1039/C7TA10136H.

[112] Z. Fu, X. Zhang, H. Zhang, Y. Li, H. Zhou, Y. Zhang, On the understandings of dielectric constant and its impacts on the photovoltaic efficiency in organic solar cells, Chin. J. Chem. 39 (2021) 381–390, https://doi.org/10.1002/cjoc.202000289.

[113] X. Liu, B. Xie, C. Duan, Z. Wang, B. Fan, K. Zhang, B. Lin, F.J.M. Colberts, W. Ma, R.A.J. Janssen, F. Huang, Y. Cao, A high dielectric constant non-fullerene acceptor for efficient bulk-heterojunction organic solar cells, J. Mater. Chem. A: Mater 6 (2018) 395–403, https://doi.org/10.1039/C7TA10136H.

[114] X. Gonze, C. Lee, Dynamical matrices, Born effective charges, dielectric permittivity tensors, and interatomic force constants from density-functional perturbation theory, Phys. Rev. B 55 (1997) 10355–10368, https://doi.org/10.1103/physrevb.55.10355.

[115] G. Murtaza Hayatullah, S. Muhammad, S. Naeem, M.N. Khalid, A. Manzar, Physical properties of $CsSnM_3$ (M = Cl, Br, I): a first principle study, Acta Phys Pol A 124 (2013) 102–107, https://doi.org/10.12693/APhysPolA.124.102.

[116] X. Liu, B. Xie, C. Duan, Z. Wang, B. Fan, K. Zhang, B. Lin, F.J.M. Colberts, W. Ma, R.A.J. Janssen, F. Huang, Y. Cao, A high dielectric constant non-fullerene acceptor for efficient bulk-heterojunction organic solar cells, J. Mater. Chem. A: Mater 6 (2018) 395–403, https://doi.org/10.1039/C7TA10136H.

[117] J. Wang, Dependence of elastic stiffness on electronic band structure of nanolaminate and ceramics, Y.Z.-P.R. B, undefined, APS 69 (2004), https://doi.org/10.1103/PhysRevB.69.214111, 2004.

[118] Minhajul Islam, Md Abdur Rob Sheikh, A comprehensive DFT study on the physical properties of XCrAl (X= Fe, Co, Ni, Cu) half-Heusler alloys for applications in high-temperature technology, Phys. B Condens. Matter 668 (2023) 415244, https://doi.org/10.1016/j.physb.2023.415244.

[119] F.D. Murnaghan, Finite deformations of an elastic solid, Am. J. Math. 59 (1937) 235–260, https://doi.org/10.2307/2371405.

[120] K. Ephraim Babu, N. Murali, K. Vijaya Babu, Paulos Taddesse Shibeshi, V. Veeraiah, Structural, elastic, electronic, and optical properties of cubic perovskite $CsCaCl_3$ compound: an ab initio study, Acta Phys. Pol., A 125 (2014) 1179–1185, https://doi.org/10.12693/APhysPolA.125.1179.

[121] M. Born, On the stability of crystal lattices. I, Math. Proc. Camb. Phil. Soc. 36 (1940) 160–172, https://doi.org/10.1017/S0305004100017138.

[122] Jahid Kabir Rony, Mohammad Nazmul Hasan, Md NJ. Rifat, Md Saiduzzaman, Minhajul Islam, Pressure-induced DFT evaluation of MSnI3 (M= K, Rb) perovskites for electronic phase transition and enhanced optoelectronic utilization, Computational and Theoretical Chemistry 1233 (2024) 114512, https://doi.org/10.1016/j.comptc.2024.114512.

[123] Ovijit Das, Mohammad Nazmul Hasan, Pallab Kumar Karmaker, Md Saiduzzaman, Minhajul Islam, Investigation of high-pressure effect on the physical properties of $FrNBr_3$ (N = Ca, Sr) non-toxic halide perovskites, Mater. Sci. Semicond. Process. 174 (2024) 108252, https://doi.org/10.1016/j.mssp.2024.108252.

[124] V.V. Brazhkin, A.G. Lyapin, S.v. Popova, Y.V. Antonov, Y.A. Kluev, A.M. Naletov, Elastic constants and elastic moduli of metals and insulators, Reference Book 7 (1982) 989–991, https://doi.org/10.4131/JSHPREVIEW.7.989.

[125] S.F. Pugh, XCII. Relations between the elastic moduli and the plastic properties of polycrystalline pure metals, London, Edinburgh Dublin Phil. Mag. J. Sci. 45 (1954) 823–843, https://doi.org/10.1080/14786440808520496.

[126] H. Fu, D. Li, F. Peng, T. Gao, X. Cheng, Ab initio calculations of elastic constants and thermodynamic properties of NiAl under high pressures, Comput. Mater. Sci. 44 (2008) 774–778, https://doi.org/10.1016/J.COMMATSCI.2008.05.026.

[127] H. Ledbetter, A. Migliori, A general elastic-anisotropy measure, J. Appl. Phys. 100 (2006) 063516, https://doi.org/10.1063/1.2338835.

[128] S.I. Ranganathan, M. Ostoja-Starzewski, Universal elastic anisotropy index, Phys. Rev. Lett. 101 (2008) 055504, https://doi.org/10.1103/PHYSREVLETT.101.055504/FIGURES/2/MEDIUM.

[129] C.M. Zener, S. Siegel, Elasticity and Anelasticity of metals, J. Phys. Colloid Chem. 53 (2002), https://doi.org/10.1021/J150474A017, 1468–1468.

[130] C.M. Kube, Elastic anisotropy of crystals, AIP Adv. 6 (2016) 095209, https://doi.org/10.1063/1.4962996.

[131] I. Hamideddine, N. Tahiri, O. El Bounagui, H. Ez-Zahraouy, Ab initio study of structural and optical properties of the halide perovskite KBX_3 compound, J. Korean Ceram. Soc. 59 (2022) 350–358, https://doi.org/10.1007/s43207-021-00178-6.

[132] H. Zitouni, N. Tahiri, O. El Bounagui, H. Ez-Zahraouy, How the strain effects decreases the band gap energy in the CsPbX3 perovskite compounds? Phase Transitions 93 (2020) 455–469, https://doi.org/10.1080/01411594.2020.1746964.

[133] A. El Badraoui, S. Dahbi, N. Tahiri, O. El Bounagui, H. Ez-Zahraouy, A DFT study of the electronic structure, optical and thermoelectric properties of perovskite $CsSnBr_3$ compound under strains effect: photovoltaic applications, Mod. Phys. Lett. B 38 (2024) 2350237, https://doi.org/10.1142/S0217984923502378.

[134] Mudasser Husain, Nasir Rahman, Hind Albalawi, Safa Ezzine, Mongi Amami, Zaman Tahir, Altaf Ur Rehman, et al., Examining computationally the structural, elastic, optical, and electronic properties of $CaQCl_3$ (Q= Li and K) chloroperovskites using DFT framework, RSC Adv. 12 (2022) 32338–32349, https://doi.org/10.1039/D2RA05602J.

[135] Mudasser Husain, Nasir Rahman, Mongi Amami, Zaman Tahir, Mohammad Sohail, Rajwali Khan, Abid Ali Khan, et al., Predicting structural, optoelectronic and mechanical properties of germanium based $AGeF_3$ (A= Ga and In) halides perovskites using the DFT computational approach, Opt. Quant. Electron. 55 (2023) 536, https://doi.org/10.1007/s11082-023-04796-8.

[136] Mudasser Husain, Hind Albalawi, Maryam Al Huwayz, Noor alhuda Al Saqri, Rajwali Khan, Nasir Rahman, Computational insight into the fundamental physical properties of ternary $ABCl_3$ chloroperovskites compounds using the DFT approach, Phys. Scripta 98 (2023) 105935, https://doi.org/10.1088/1402-4896/acf695.

[137] Jaffer Saddique, Mudasser Husain, Nasir Rahman, Rajwali Khan, Anwar Iqbal, Mohammad Sohail, Shaukat Ali Khattak, et al., Modeling structural, elastic, electronic and optical properties of ternary cubic barium based fluoroperovskites $MBaF_3$ (M= Ga and In) compounds based on DFT, Mater. Sci. Semicond. Process. 139 (2022) 106345, https://doi.org/10.1016/j.mssp.2021.106345.